

Numerical Study of Metalens

by

Yueheng Peng

**A thesis submitted in partial fulfillment
of the requirements for the degree of
Master of Science in Engineering
(Electrical Engineering)
in the University of Michigan-Dearborn
2018**

Master's Thesis Committee:

**Professor Yasha Yi, Chair
Professor Weidong Xiang
Associate Professor Nilay Chakraborty**

ACKNOWLEDGEMENTS

Here I want to express my most sincere gratitude to Professor Yasha Yi, my thesis advisor, for his kindness and patient help. Without his help, this thesis definitely cannot be completed.

Also, I want to show my appreciation to my colleague Mao Ye, Wei Guo, Dachuan Wu, Xiao Wang and Xiaopeng Guo for their help and company during the days at UM-Dearborn.

At last, thank all the people who ever gave me a hand during the research work in this year.

TABLE OF CONTENTS

ACKNOWLEDGEMENTS	ii
LIST OF FIGURES	v
ABSTRACT.....	viii
Chapter I Introduction and Basic Theory of Metalens.....	1
1.1 Introduction of Negative Refractive Index	1
1.2 Basic Instruction of Metalens	3
Chapter II Deep Understanding and Multiple Theory of Metalens	6
2.1 Discretization of Conventional Lens	6
2.2 Theory of Metalens Derived from Conventional Lens	10
2.3 Explanation of Metalens Mechanism by Generalized Snell's Laws	14
Chapter III Two-Dimensional & Three-Dimensional Metalens	20
3.1 Explanation and Steps of Metalens Design	20
3.2 Simulation and Analysis of Two-Dimensional Lens.....	22
3.3 Design and Optical Characterization of Three-Dimensional Lens	27
Chapter IV Linear Polarization Distinguishing Metalens in Visible	34
4.1 Introduction of Polarization	34
4.2 Design Strategy of Linear Polarization Distinguishing Metalens.....	35
4.3 Simulation and Discussion.....	39
4.4 Fabrication and Characterization	41
4.5 Conclusion	44
Chapter V Design and Simulation about 3D Metalens with Different Shapes of Focus	45

5.1 Straight-Line Focus.....	45
5.2 Several Methods to Approach ‘M’ Structure Gradually	47
5.3 Two kinds of Arcuated Focus.....	53
Chapter VI Conclusion	56
REFERENCES	57
Appendix: Publications.....	59

LIST OF FIGURES

Fig. 1.1 Illustration of Refraction	1
Fig. 1.2 Illustration of Negative Refraction	2
Fig. 1.3 A titanium dioxide metamaterial lens	3
Fig. 1.4 Image courtesy of Jared Sisler/Harvard SEAS.....	3
Fig. 1.5 Limitation of traditional lens	4
Fig. 2.1 Basic structure of traditional lens	6
Fig. 2.2 Basic structure of traditional lens	7
Fig. 2.3 A sinusoidal EM wave	8
Fig. 2.4 An assumption of flat surface lens.....	10
Fig. 2.5 Basic photolithography process steps.....	11
Fig. 2.6 Structure of new phase shifter	12
Fig. 2.7 Schematic of Metalens.....	13
Fig. 2.8 Illustration of Refraction	14
Fig. 2.9 Schematic used to derive the generalized Snell's law	15
Fig. 2.10 Illustration of direction control.....	17
Fig. 2.11 Design of Metalens by Generalized Snell's Law	18
Fig. 2.12 Design of Metalens.....	18
Fig. 3.1 Schematic of Metalens and Phase Shifter.....	20
Fig. 3.2 Schematic of RCWA Simulation	21
Fig. 3.3 Phase diagram for Si ₃ N ₄ phase shifter.....	23
Fig. 3.4 Relationship between Phase shift and Width.....	24

Fig. 3.5 Field distribution and Focus efficiency of metalens.....	25
Fig. 3.6 Comparison between 360nm pitch size and 220nm pitch size.....	26
Fig. 3.7 Different kind of phase shifters	27
Fig. 3.8 Design of Metalens (10 $\mu\text{m}\times 10 \mu\text{m}$)	28
Fig. 3.9 Design of Grating lens (10 $\mu\text{m}\times 10 \mu\text{m}$)	29
Fig. 3.10 Field distribution of 3D simulation	30
Fig. 3.11 Nine groups of lenses.....	30
Fig. 3.12 Optical Characterization	31
Fig. 3.13 Focus image received by camera.....	32
Fig. 4.1 Design strategy of linear polarization distinguishing metalens.....	36
Fig. 4.2 Phase and Transmission Diagram for polarization phase shifters	37
Fig. 4.3 Field distribution at cross-section $x=0$ of the lens.....	39
Fig. 4.4 Field distribution of lens.....	40
Fig. 4.5 SEM image of polarization distinguishing lens.....	41
Fig. 4.6 Illustration of characterization system.....	42
Fig. 4.7 Optical characterization of linear polarization distinguishing metalens	43
Fig. 5.1 Schematic of straight-line focus	45
Fig. 5.2 Schematic and Field distribution of straight-line focus metalens.....	46
Fig. 5.3 ‘M’ structure	47
Fig. 5.4 Schematic of focus shift in X-axis direction	47
Fig. 5.5 Schematic of focus shift in X-axis direction	48
Fig. 5.6 Schematic of discretization method.....	49
Fig. 5.7 Simulation of discretization method.....	50
Fig. 5.8 Simulation of discretization method.....	51
Fig. 5.9 Simulation of space saving design.....	52

Fig. 5.10 Schematic of arcuated focus lens.....	53
Fig. 5.11 Simulation of arcuated focus lens.....	54
Fig. 5.12 Design and Simulation of arcuated focus lens.....	55

ABSTRACT

This thesis introduces a research project completed by Yueheng Peng. All the study are based on numerical simulation method. The first part described about the history of negative refractive index material, including difference with conventional materials and recent advances in metamaterials research and discuss the potential that these materials may hold for realizing new phenomena and application. Secondly, our own deep understanding and theory of metalens is proposed and explained clearly. The third part illustrated how to design 2-D & 3-D metalens and simulation results, at different numerical aperture, we can achieve efficiency more than 60%. Then we will talk about the optical characterization. With the help of camera (DCC3240C, Thorlabs), we can observe the characterized field distribution on the plane of focus. The last two parts are about Linear Distinguishing Metalens and Metalens providing focus in different shapes. In this study, we propose a metalens that integrates the function of concentrating lens and linear polarizer. All the results are based on Finite Difference Time Domain (FDTD) simulation method in electromagnetism. The entire thesis is structured as following: 1. Introduction and Basic Theory of Metalens; 2. Deep understanding and multiple theories of metalens. 3. 2-D & 3-D lens: Design and Optical Characterization; 4. Linear Distinguishing Metalens; 5. 3-D Metalens with Focus in Different Shapes.

Chapter I Introduction and Basic Theory of Metals

1.1 Introduction of Negative Refractive Index

As we know, the positive refractive index material can be described by the Snell's Law. When dielectric 1 and dielectric 2 are all positive refractive index material ($\epsilon > 0, \mu > 0$). The relationship between incident angle θ_i and refraction angle θ_t can be described by Snell's Law which relates the angles of incidence and refraction to the refractive indices of the media.

$$\frac{\sin\theta_i}{\sin\theta_t} = \frac{n_2}{n_1} \quad (1.1.1)$$

The ratio of the speed of light in free space to its speed in a medium is called the

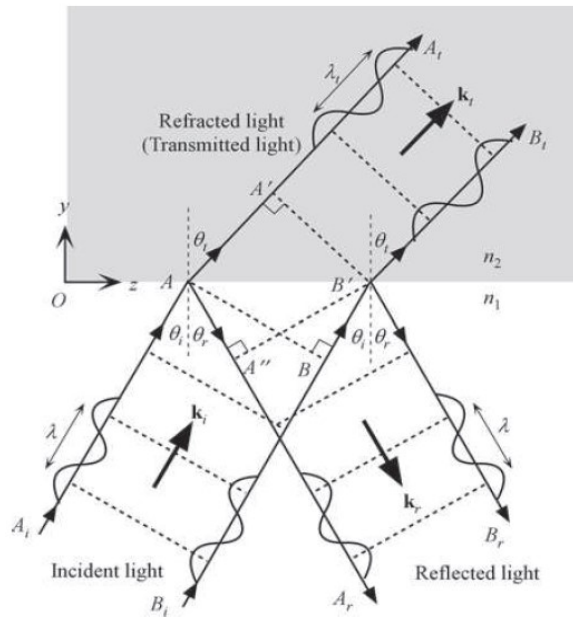


Fig. 1.1 Illustration of Refraction

refractive index n of the medium, that is,

$$n = \frac{c}{V} = \sqrt{\epsilon} \quad (1.1.2)$$

In a dielectric medium of relative permittivity ϵ_r , the phase velocity V is given by

$$V = \frac{1}{\sqrt{\epsilon\mu}} \quad (1.1.3)$$

In the derivation of Snell's Law, $n^2 = \epsilon\mu$, $n = \pm\sqrt{\epsilon\mu}$. So, what will happen at the condition $n = -\sqrt{\epsilon\mu}$? Up till now, there is no natural negative refractive index material founded in the world. So, this equation was not mentioned a lot by people all along.

This assumption was proposed by V.G.Veselago in 1968. His ignition point was the pioneering 1968 paper on the electrodynamics of isotropic substances with simultaneously

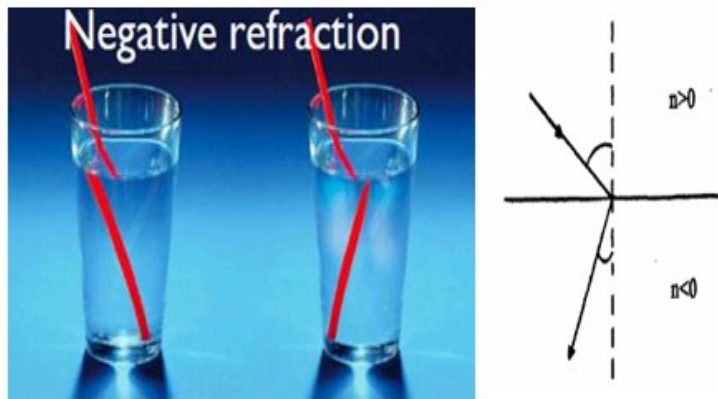


Fig. 1.2 Illustration of Negative Refraction

negative values of dielectric constant and magnetic permeability. Within this beautiful work, Veselago categorically stated that there had not been, so far, any experiment in which a substance such as this could even be identified.

Although we can't find negative refractive index material in nature, this kind of material can be made artificially. John Pendry was the first to identify a practical way to make a negative refractive index metamaterial. Pendry's idea was that metallic wires aligned along the direction of a wave could provide negative permittivity (dielectric function $\epsilon < 0$). Natural materials (such as ferroelectrics) display negative permittivity; the challenge was achieving negative permeability ($\mu < 0$). In 1999 Pendry demonstrated that a split ring (C shape) with its axis placed along the direction of wave propagation could do so. In the same paper, he showed that a periodic array of wires and rings could give rise to a negative refractive index. Pendry also proposed a related negative-permeability design, the Swiss roll. This is called metamaterial now.

A metamaterial (from the Greek word $\mu\epsilon\tau\acute{\alpha}$ meta, meaning "beyond") is a material

engineered to have a property that is not found in nature. They are made from assemblies of multiple elements fashioned from composite materials such as metals or plastics. The materials are usually arranged in repeating patterns, at scales that are smaller than the wavelengths of the phenomena they influenced. Metamaterials derive their properties not from the properties of the base materials, but from their newly designed structures.

1.2 Basic Instruction of Metalens

With the application of metamaterial, people want to use nanostructures to focus light. A

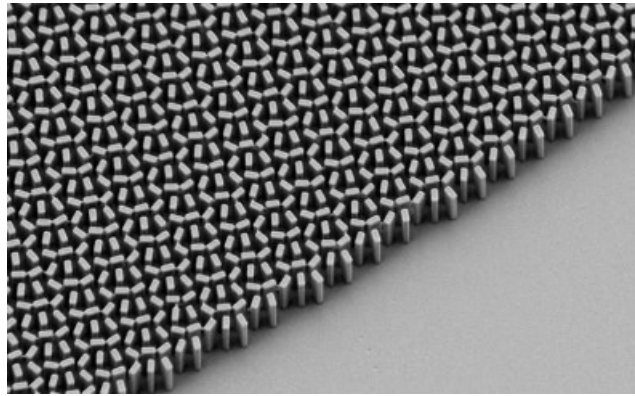


Fig. 1. 3 A titanium dioxide metamaterial lens
(Metamaterial lens is thinner than the light it bends and focuses)

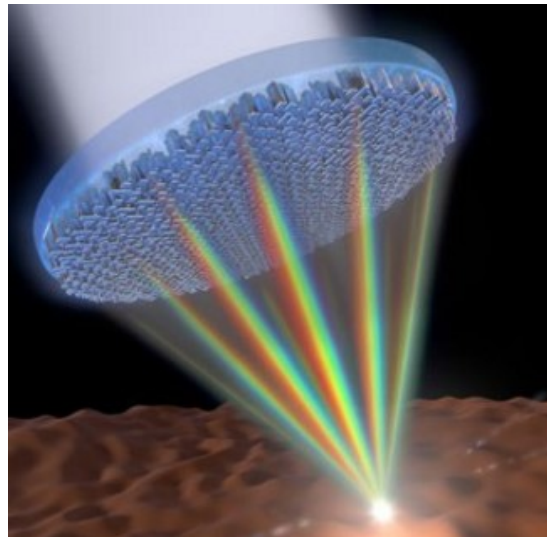


Fig. 1. 4 Image courtesy of Jared Sisler/Harvard SEAS

flat structures comprised by multiple nanostructures, each nanostructure is used to control the radiation pattern of an incident electromagnetic wave, making the wavefront of the light focusing at a point like the function of conventional lens.

Here, the flat structure is called Metasurface, a new kind of optically thin subwavelength structured interface (subwavelength $\ll\lambda$, the size of nanostructures on metasurface is much smaller than wavelength). The metalenses' ideal structure and visual effect are shown in Fig. 1. 4.

Metalenses have advantages over traditional lenses. Conventional cameras and optical instruments use multiple curved lenses of different thicknesses and materials to correct these aberrations, which, of course, adds to the bulk of the device. Numerical aperture of an optical system such as an objective lens is defined by

$$NA = n \sin\theta \quad (1.2.1)$$

In figure 1.5, f is the focal length of the focus at F1. In free space $n = 1$, $NA = \sin\theta$, so the shorter the focal length, the larger the angle θ , and the NA can be infinitely close to 1. So, by increasing the NA, the focus will be gradually moved from F1 to F3. In the condition that the focus is at F3, there should be some overlap between the propagation of the light and the surface of the lens which is impossible. In order to solve this problem and achieve high NA lens, traditional optical instruments are composed by multiple curved lenses in series which costs a lot of space in device. In this case, Metalens is promising to revolutionize optics by replacing the bulky, curved lenses currently used in optical devices by a simple, flat surface.

The required phase profile to achieve diffraction-limited focusing for collimated incident

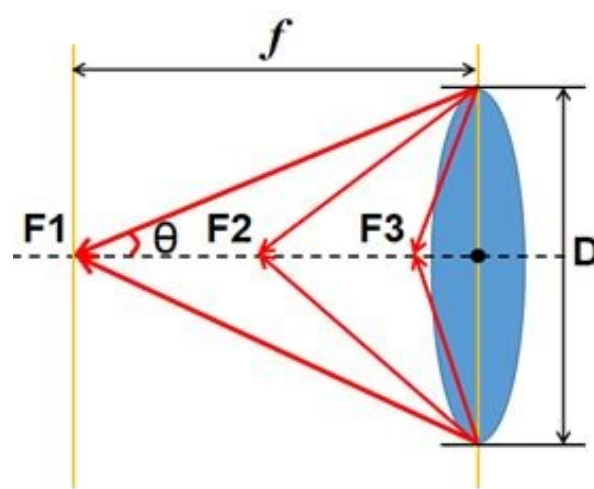


Fig. 1. 5 Limitation of traditional lens

light is that,

$$\varphi(x) = \varphi(0) - \frac{2\pi}{\lambda}(\sqrt{x^2 + f^2} - f) \quad (1.2.2)$$

where λ is wavelength, f is focal length, x is the distance from the center of the lens to a random position on the surface, and $\varphi(0)$ is a reference phase, which is chosen to be wavelength dependent. $\varphi(x) - \varphi(0)$ is also called phase shift or phase jump. This equation describes the requirement of the phase shift as a function of position.

Chapter II Deep Understanding and Multiple Theory of Metalens

2.1 Discretization of Conventional Lens

In order to have a better understanding of metalens, we have made some study on conventional lens. Conventional lenses are classified by the curvature of the two optical surfaces. A lens is biconvex (or double convex, or just convex) if both surfaces are convex, shown in Fig. 2. 1. If one of the surfaces is flat, the lens is plano-convex or plano-concave depending on the curvature of the other surface. A lens with one convex and one concave side is convex-concave or meniscus. The distance from the lens to the spot is the focal length of the lens, which is commonly abbreviated f in diagrams and equations.

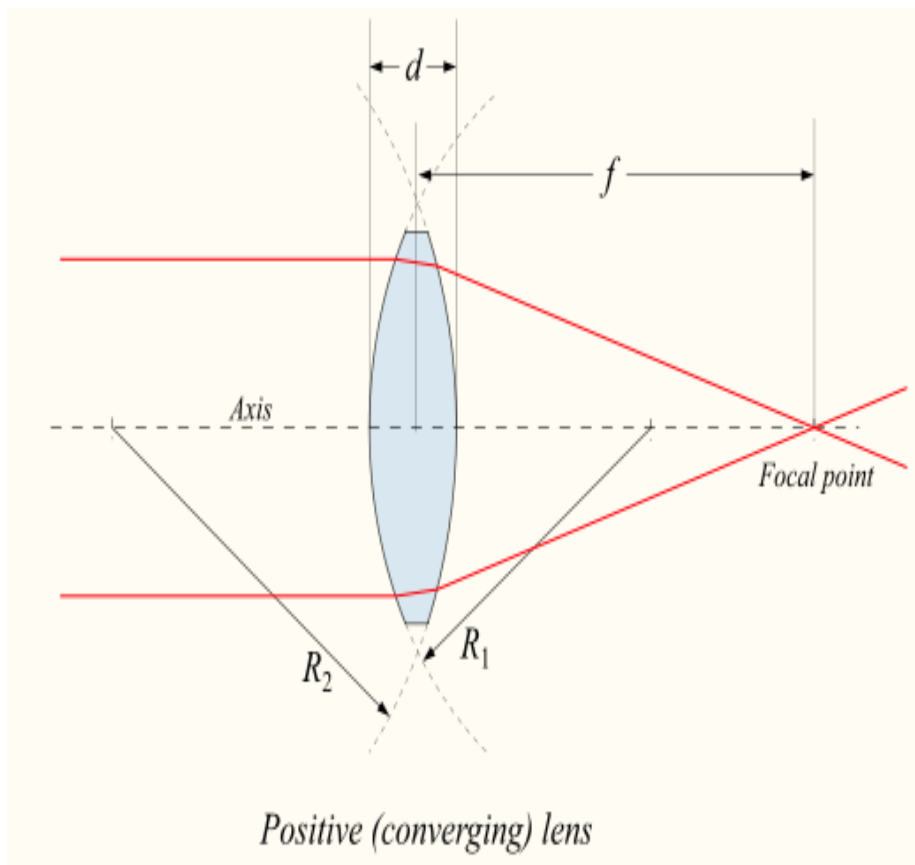


Fig. 2.1 Basic structure of traditional lens

We all know that a lens in air can focus a collimated beam travelling along the lens axis to a spot (called focal point) at a distance f from the lens. The general explanation is that refraction happens at the two interfaces of the lens. Here we applied discretization method to analyze the focus phenomenon of conventional Lens. To simplify this model, we made some analysis about plano-convex lens in Fig. 2.2(We discretized this lens to many rectangles with different height and the same width). In this figure, f is focal length, Y is the distance from the C to D (D is a random position), and L is the distance from A to O. Assuming a planewave incident light with wavelength λ , the red lines and the green lines showed two different light propagation (propagation A & propagation B) focused at the focal point F respectively.

We can treat light as an electromagnetic (EM) wave with time-varying electric and

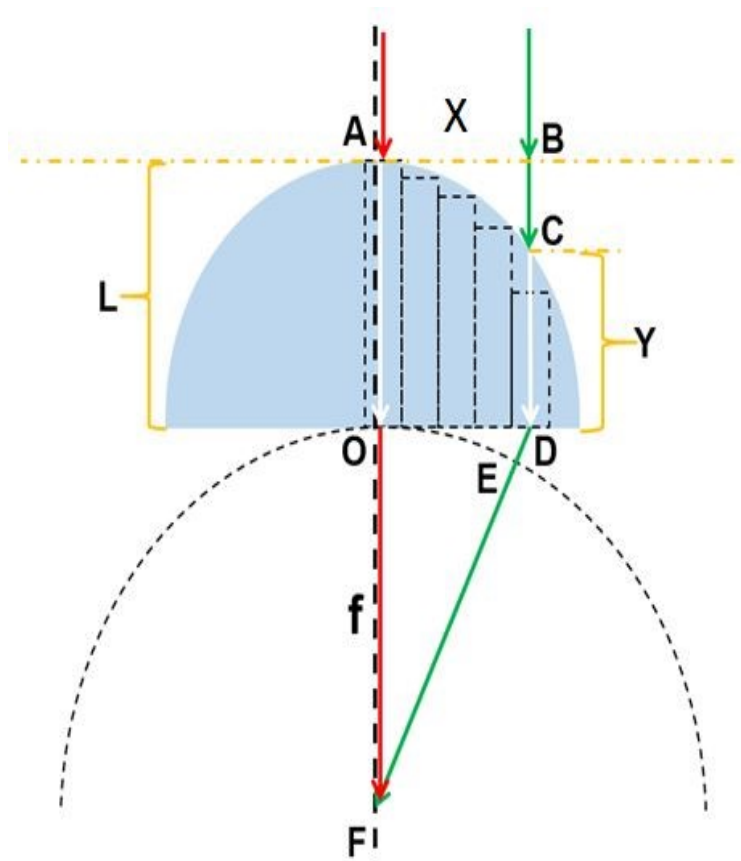


Fig. 2. 2 Basic structure of traditional lens

magnetic fields, E_x and B_y , respectively, which are propagating through space in such a way that they are always perpendicular to each other and the direction of propagation z as

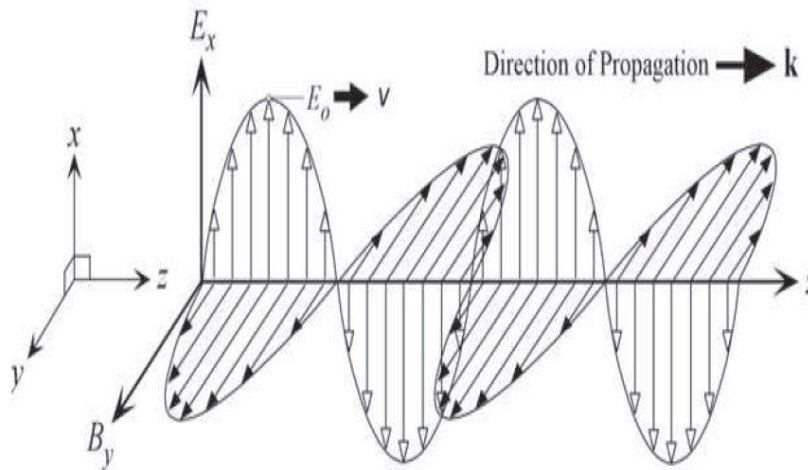


Fig. 2. 3 A sinusoidal EM wave

illustrated in Figure 2.3. The simplest traveling wave is a sinusoidal wave that, for propagation along z , has the general mathematical form

$$E_x = E_0 \cos(\omega t - \mathbf{k}z + \varphi) \quad (2.1.1)$$

in which E_x is the electric field at position z at time t , k is the propagation constant given by $2\pi/\lambda$, where λ is the wavelength, ω is the angular frequency, E_0 is the amplitude of the wave, and φ is a phase constant, which accounts for the fact that at $t = 0$ and $z = 0$; E_x may or may not necessarily be zero depending on the choice of original phase constant. The argument $(\omega t - \mathbf{k}z + \varphi)$ is called the phase of the wave and denoted by φ . A wavefront of a plane wave is an infinite plane perpendicular to the direction of propagation as shown in Figure 2.3. We indicate the direction of propagation with a vector \mathbf{k} , called the wave vector (or propagation vector), whose magnitude is the propagation constant, $k = 2\pi/\lambda$ ($k_{\text{medium}} = nk$). The \mathbf{k} is perpendicular to constant phase plane.

In order to obtain a focus at F, we need to keep the wavefronts arriving F always with a same phase. In equation 2.1.1, the phase of a wavefront is described as $(\omega t - \mathbf{k}z + \varphi)$. The light from the source at the top of this device is a plane wave with λ . So, the light through propagation A and B are both with the same angular frequency ω . And the light propagation illustrated by green line and red line in Fig. 2. 2 are generated by a same light source, so the wavefront at point A and point B have the same original phase constant φ . So, we just need to pay more attention on the phase shift described as $(-\mathbf{k}z)$ now ($-\mathbf{k}z$ talks about the light propagation).

For propagation A, the phase shift can be described as:

$$\text{Phase shift A} = -k_{\text{medium}} \times \text{AO} - k \times \text{OF} = -k_{\text{medium}} \times L - k \times f \quad (2.1.2)$$

For propagation B, the phase shift can be described as:

$$\text{Phase shift B} = -k \times \text{BC} - k_{\text{medium}} \times \text{CD} - k \times \text{DF} = -k \times (L - Y) - k_{\text{medium}} \times Y - k \times (DE + f) \quad (2.1.3)$$

Assume that Phase shift A = Phase shift B (the condition to achieve a focus at the focal point), we can obtain this equation 2.1.4:

$$-k_{\text{medium}} \times L - k \times f = -k \times (L - Y) - k_{\text{medium}} \times Y - k \times (DE + f) \quad (2.1.4)$$

After six steps of simplification, the relationship of the phase of the wavefront at D and O respectively can be illustrated by equation 2.1.5:

$$-k_{\text{medium}} \times L = -k \times (L - Y) - k_{\text{medium}} \times Y - k \times DE$$

$$k_{\text{medium}} \times (Y - L) = -k \times (L - Y) - k \times DE$$

$$k_{\text{medium}} \times (Y - L) + k \times (L - Y) = -k \times DE$$

$$(k_{\text{medium}} - k) \times (Y - L) = -k \times DE$$

$$(nk - k) \times (Y - L) = -k \times DE$$

$$k(n - 1) \times (L - Y) = k \times DE$$

$$(2\pi/\lambda)(n - 1)(L - Y) = 2\pi \frac{\sqrt{f^2 + X^2} - f}{\lambda} \quad (2.1.5)$$

Now we just consider about the phase of the wavefront at point D and point O, and it can be explained by

$$\varphi(D) - \varphi(O) = k \times DE = 2\pi \frac{\sqrt{f^2 + X^2} - f}{\lambda} \quad (2.1.6)$$

Combine equation (2.1.5) and equation (2.1.6), then we can obtain

$$\varphi(D) - \varphi(O) = (2\pi/\lambda)(n - 1)(L - Y) = 2\pi \frac{\sqrt{f^2 + X^2} - f}{\lambda} \quad (2.1.7)$$

Here $\varphi(D)$ and $\varphi(O)$ are the phase of wavefront at point D and point O respectively. According to equation 2.1.7, we can observe that the shorter the Y (the thickness of the lens at a certain point where OD=X), the larger the phase difference between $\varphi(D)$ and $\varphi(O)$.

In this case, it is clear that the mechanism of conventional lens is to change the thickness of lens to satisfy the requirement of phase difference between D and O (the requirement of phase difference is just depended on focal length and the position of D).

2.2 Theory of Metalens Derived from Conventional Lens

As we mentioned in chapter 1, it is difficult for traditional lens to achieve high NA because of the curved screen. In order to solve the problem given by the curve, we wanted to design a lens which has a flat surface.

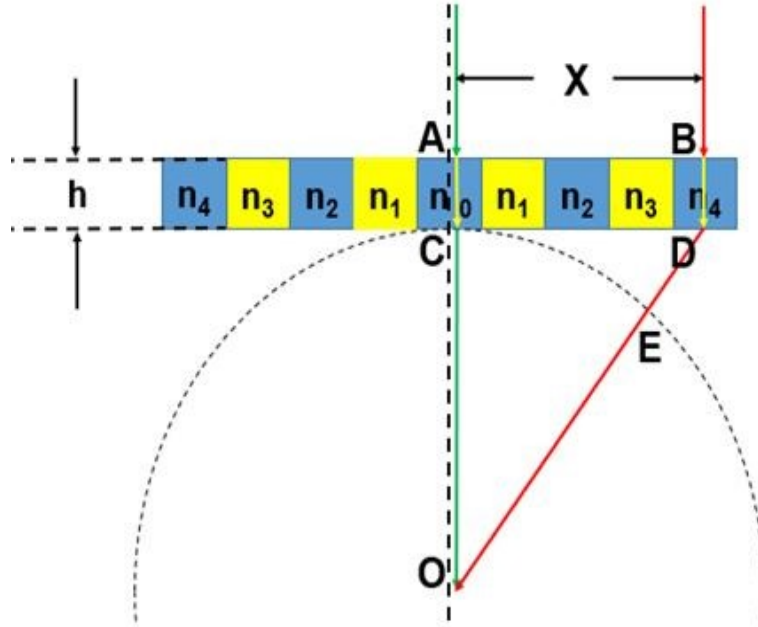


Fig. 2. 4 An assumption of flat surface lens

As shown in Fig 2.4, we use material with different refractive index to replace the function given by changing the thickness of the lens. Here n_0, n_1, n_2, n_3, n_4 are the value of different refractive index of each rectangular part (we define these rectangular part as phase shifter, because it provides the function of tuning the phase of wavefront). And the refractive index of these rectangle parts at each symmetric position keeps the same value, since this lens is symmetric. Then we can do the similar analysis of the phase shift for propagation ACO and propagation BDO like the analysis of conventional lens.

For propagation A, the phase shift can be described as:

$$\text{Phase shift A} = -k \times n_0 \times AC - k \times CO = -k \times (n_0 \times h + f) \quad (2.2.1)$$

For propagation B, the phase shift can be described as:

$$\text{Phase shift B} = -k \times n_4 \times BD - k \times DO = -k \times (n_4 \times h + f + DE) \quad (2.2.2)$$

Assume that Phase shift A = Phase shift B (the condition to achieve a focus at the focal point), we can obtain this equation 2.2.3:

$$-k(n_0 \times h + f) = -k \times (n_4 \times h + f + DE) \quad (2.2.3)$$

After three steps of simplification, the relationship between the phase of the wavefront at D and C respectively can be illustrated by equation 2.2.4:

$$-k \times (n_0 \times h) = -k \times (n_4 \times h + DE)$$

$$-k \times (n_0 \times h - n_4 \times h) = -k \times DE$$

$$k \times (n_0 - n_4) \times h = k \times DE$$

$$\left(\frac{2\pi}{\lambda}\right) (n_0 - n_4)h = 2\pi \frac{\sqrt{f^2 + X^2} - f}{\lambda} \quad (2.2.4)$$

Now we just consider about the phase of the wavefront at point D and point C, and it can be explained by

$$\varphi(D) - \varphi(C) = k \times DE = 2\pi \frac{\sqrt{f^2 + X^2} - f}{\lambda} \quad (2.2.5)$$

Combine equation (2.2.4) and equation (2.2.5), then we can obtain

$$\varphi(D) - \varphi(C) = \left(\frac{2\pi}{\lambda}\right) (n_0 - n_4)h = 2\pi \frac{\sqrt{f^2 + X^2} - f}{\lambda} \quad (2.2.6)$$

This equation described about the phase difference between the phase of wavefront at position D and position C. And the value of this phase difference is $2\pi \frac{\sqrt{f^2 + X^2} - f}{\lambda}$, which is a function with X as its independent variable. Assuming n_0 and h are constant, in order to satisfy this value of phase difference, we just need to change the value of n_4 at each position X. So, we can design a flat lens with a thickness of h by changing the refractive index of each

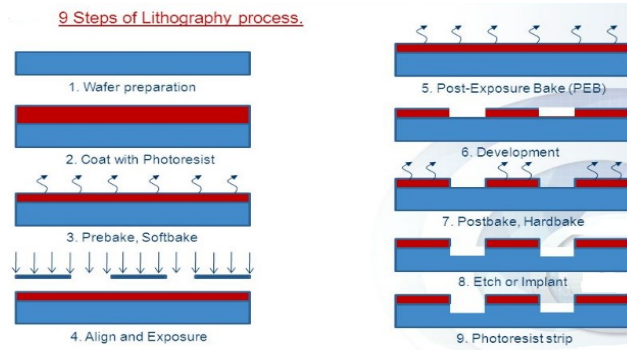


Fig. 2. 5 Basic photolithography process steps

phase shifter at their corresponding position X.

This method seems to be feasible but it has limitations in fabrication and cost. There are many steps in fabrication including photoresist coating, exposure, development, hardbake and etch etc., as shown in Fig 2.5. Each step costs long time and need a help with a precise mask.

The fabrication is processing upwardly layer by layer and the feature size is nanometer level. In this case, it is difficult to fabricate each phase shifter with different refractive index (different material).

So, we design a periodical and single material structure to replace the structure composed by rectangular phase shifters made by different refractive index material. Each

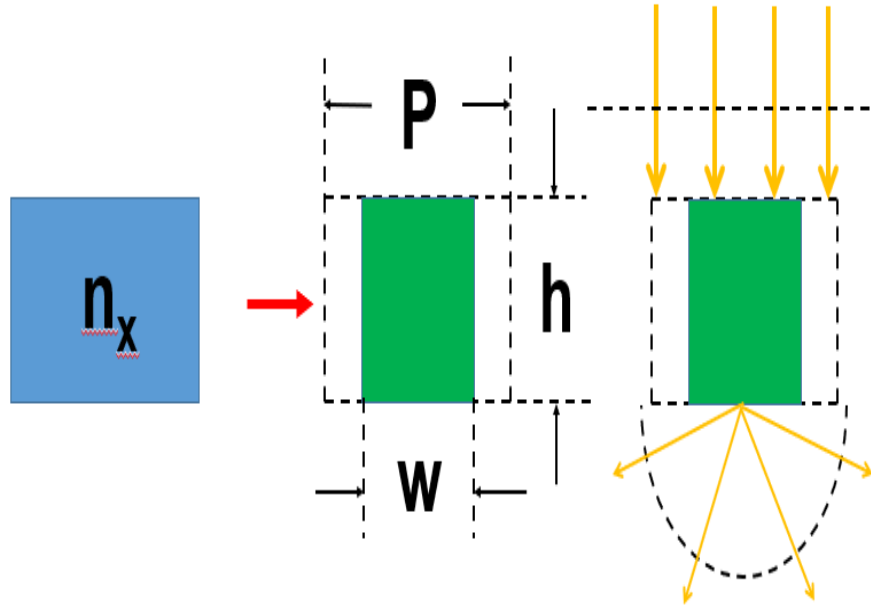


Fig. 2. 6 Structure of new phase shifter

phase shifter in Fig 2.4 is replaced by a new kind of phase shifter shown in Fig 2.6. In this figure, P is the length of each period of each phase shifter, h is the height of these phase shifters which is the same as the structure in Fig 2.4, and W is the width of the structure for each phase shifter. Here, we define the ratio of W and P as fill factor (Fill Factor = W/P). Since the size of one period is less than 400nm which is less than the wavelength of the light source we applied in our design, each period of structure can be considered as a whole with a new refractive index n_{eff} (effective refractive index). According to switch the W (width) of these phase shifters, we can achieve phase shifters with different effective refractive index n_{eff} . Then we can use these phase shifters to obtain the appropriate phase shift at each position of the lens.

The Fig 2.7 shows the basic configuration of the metalens. We use phase shifters with different width but same period to achieve the function given by the design in Fig 2.4. Here each phase shifter has different width corresponding to its location. And the width of phase shifters at symmetric position keeps the same value, since this lens is symmetric. Then we can do the similar analysis of the phase shift for propagation ACO and propagation BDO just like the former analysis. The relationship of the phase can be described:

Fig. 2. 7 Schematic of Metalens

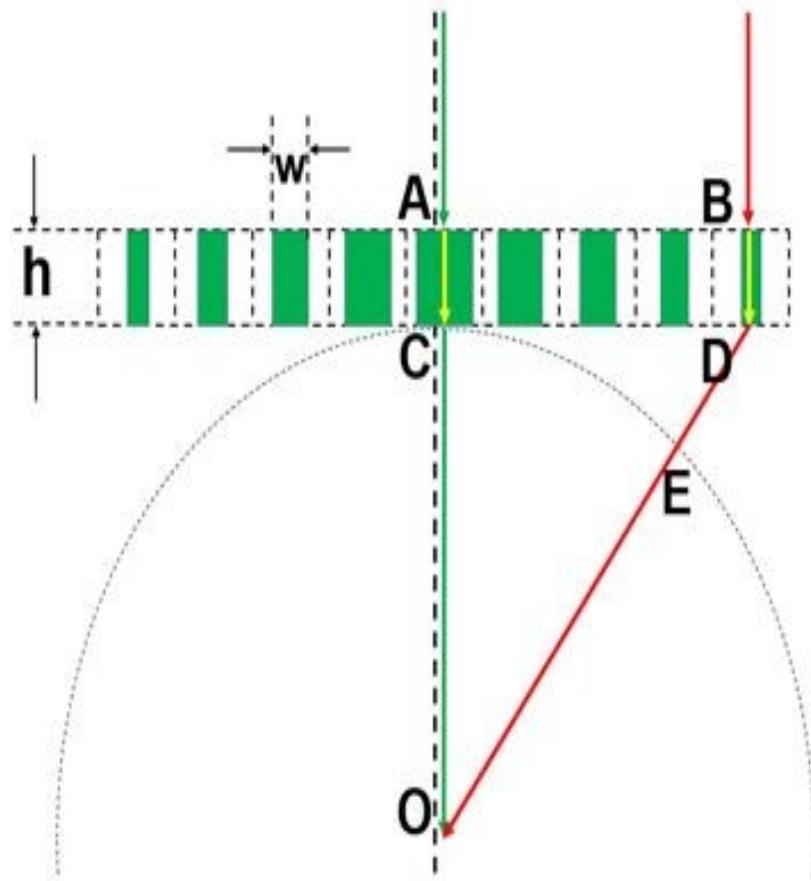


Fig. 2. 7 Schematic of Metalens

$$\varphi(D) - \varphi(C) = 2\pi \frac{\sqrt{f^2 + X^2} - f}{\lambda} \quad (2.2.7)$$

Here $\varphi(D)$ and $\varphi(C)$ are the phase of wavefront at point D and point C respectively. And f is focal length (CO=f). Equation 2.2.7 illustrated the relationship between the position (X) of the phase shifter and the phase difference can be obtained.

In this thesis, we utilized this basic schematic to design and analyze metalens.

2.3 Explanation of Metalens Mechanism by Generalized Snell's Laws

In last unit, we explained and derived our understanding of metalens, analyzing the mechanism of conventional lens and then making some modification and optimization to

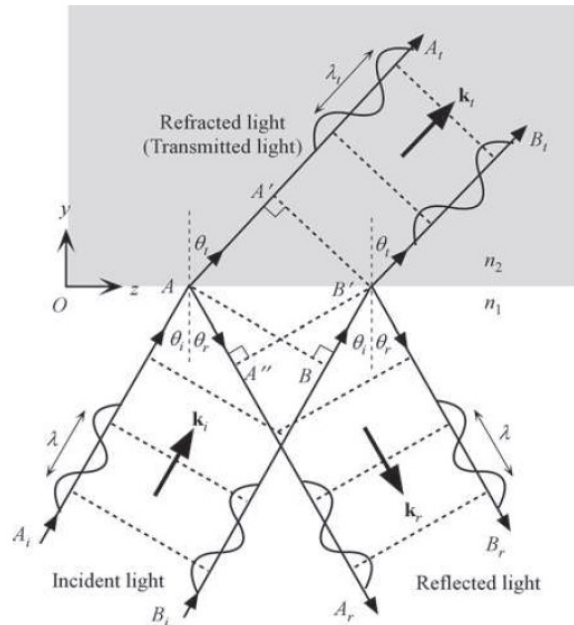


Fig. 2.8 Illustration of Refraction

complete this story. There is another leading-edge theory to provide a clear way to study metalens called Generalized Snell's Law. Inevitably, we need to mention about Snell's Law which is a basic theory of light propagation relating the angles of incidence and refraction to the refractive indices of the media.

$$\frac{\sin\theta_i}{\sin\theta_t} = \frac{n_2}{n_1} \quad (2.3.1)$$

This equation can only be established under a certain circumstance that there is no phase discontinuities at the interface.

Although Snell's Law is applicable in most cases, we don't know what will happen when there are phase discontinuities at the interface. So, we want to mention about Generalized Snell's Law of refraction and reflection which was first proposed by Nangfang Yu in 2011 with some analysis by applying Fermat's principle. Here we will derive this equation with some geometrical optics analysis and illustrate the relationship between Generalized Snell's Law and metalens, making it a full story. Consider an incident plane

wave at an angle θ_i . Assuming that the two paths (green line and blue line) are infinitesimally

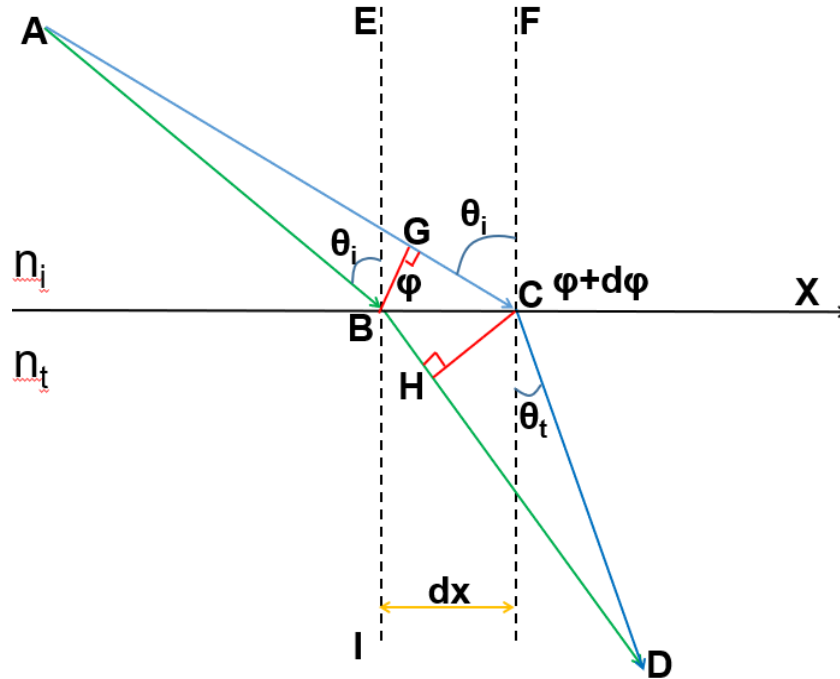


Fig. 2.9 Schematic used to derive the generalized Snell's law

close to the actual light path which is shown in Fig 2.9. Here the interface between the two media is artificially structured in order to introduce an abrupt phase shift in the propagation of light which has relationship between the position along the interface (X-axis). Φ and $\Phi+d\Phi$ are the phase discontinuities where two paths cross the artificial boundary at point B and point C respectively. θ_t is the angle of refraction; dx is the distance between two crossing point B and C which is infinitesimally short; n_i and n_t are the refractive indices of the two media; and $k_0 = 2\pi/\lambda_0$, where λ_0 is the vacuum wavelength.

Assuming the wavefront at Point A have two different directions but in phase; and the wavefront from two paths meeting at Point D are in phase. This is because the two paths are infinitesimally close to each other. So, the phase difference between them is zero. And we can describe this relationship by equation 2.3.2:

$$k_0 \times n_i \times AB + k_0 \times n_t \times BD + \Phi = k_0 \times n_i \times AC + k_0 \times n_t \times CD + \Phi + d\Phi \quad (2.3.2)$$

Here, since BC is infinitesimally short, we assume that AB equals AG and HD equals CD. After four steps of simplification, the relationship between the phase of the wavefront at B and C respectively can be illustrated by equation 2.3.3:

$$k_0 \times n_i \times AB + k_0 \times n_t \times (BH+HD) + \Phi = k_0 \times n_i \times (AG+GC) + k_0 \times n_t \times CD + \Phi + d\Phi$$

$$k_o \times n_t \times (BH+HD) + \Phi = k_o \times n_i \times GC + k_o \times n_t \times CD + \Phi + d\Phi$$

$$k_o \times n_t \times BH + \Phi = k_o \times n_i \times GC + \Phi + d\Phi$$

$$k_o \times n_t \times BH = k_o \times n_i \times GC + d\Phi$$

$$k_o \times n_t \times BC \times \cos \angle CBH = k_o \times n_i \times BC \times \cos \angle GCB + d\Phi \quad (2.3.3)$$

Since BC is infinitesimally short, we can assume that AB is parallel with AC and BD is parallel with CD. In this case, $\angle ABE$ equals $\angle ACF$ and $\angle IBD$ equals θ_t . Then we can obtain equation 2.3.4 after some equivalent substitution:

$$k_o \times n_t \times BC \times \sin \angle \theta_t = k_o \times n_i \times BC \times \sin \angle \theta_i + d\Phi$$

$$k_o \times n_t \times dx \times \sin \angle \theta_t = k_o \times n_i \times dx \times \sin \angle \theta_i + d\Phi$$

$$n_t \times \sin \angle \theta_t = n_i \times \sin \angle \theta_i + (1/k_o) \times (d\Phi/dx) \quad (2.3.4)$$

Equation 2.3.4 is called Generalized Laws of Refraction, illustrating about the relationship between the angles of incidence and refraction to the refractive indices of the media in such a condition that the phase gradient along the interface is not zero. If the phase gradient equals zero ($d\Phi/dx = 0$), it is just the same as Snell's Law in equation 2.3.1. So, Generalized Snell's Law made a more comprehensive description about the light propagation at interface than Snell's Law, like the relationship between Theory of Relativity and Newton's laws of Motion.

We can change equation 2.3.4 to another form, making each side divided by n_t . So here we come to a new form which relates the angles of refraction and incidence to the refractive indices of the media, shown in equation 2.3.5:

$$\sin \angle \theta_t = (n_i/n_t) \times \sin \angle \theta_i + (1/k_o) \times (1/n_t) \times (d\Phi/dx) \quad (2.3.5)$$

This equation illustrate that we can modify the angle of refraction by changing the phase gradient and the angle of incidence. Then we can utilize this equation to make some analysis of metalens. Since the light from the source at the top of metalens is a plane wave which has a direction perpendicular to the interface of the lens, we can assume the incident angle θ_i equals zero ($\theta_i=0$). In this case, the value of refraction angle is given by equation 2.3.6:

$$\sin \angle \theta_t = (1/k_o) \times (1/n_t) \times (d\Phi/dx) \quad (2.3.6)$$

So, we can control the refraction angle by just changing the phase gradient($d\Phi/dx$), because the n_t and k_o are both constant. As shown in Fig 2.10, the incident light is perpendicular to the

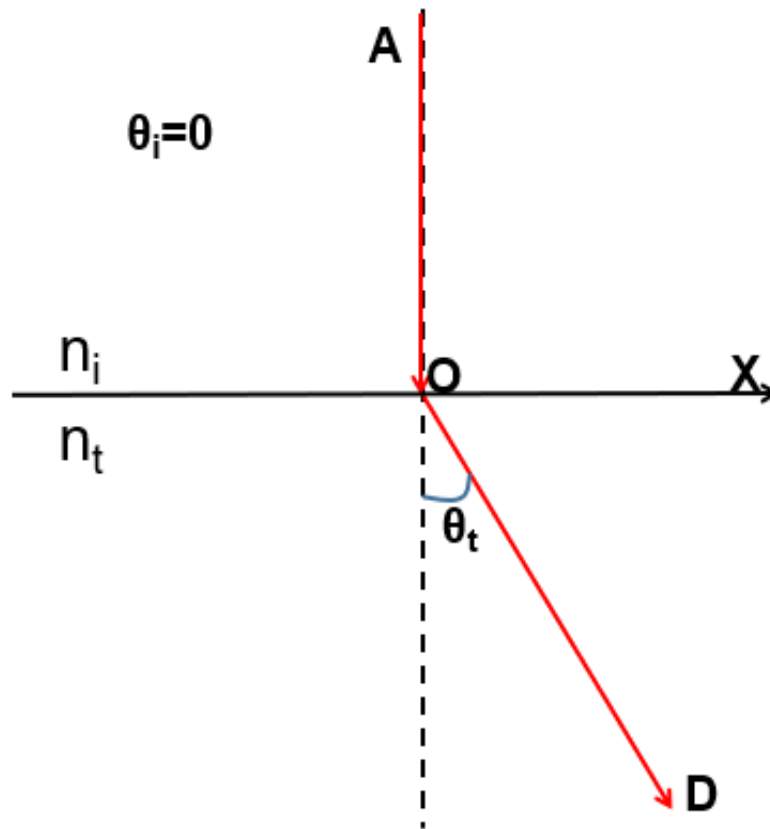


Fig. 2.10 Illustration of direction control

interface, and the value of refraction angle θ_t is a function of phase gradient. Since it is in free space, the value of n_t equals one. With this method, we can design an interface that has appropriate gradient at each position along x-axis which can provide appropriate refraction angles that makes each light focus at one certain point, as shown in Fig 2.11. In this schematic, every light propagation focus at point D. We can easily get each refraction angle by geometric calculation and then figure out the phase gradient at each position along the interface by equation 2.3.6.

It seems that this design achieves the same function as Metalens. So, the question now is how to realize this interface and how to obtain appropriate phase gradient at certain position. Is

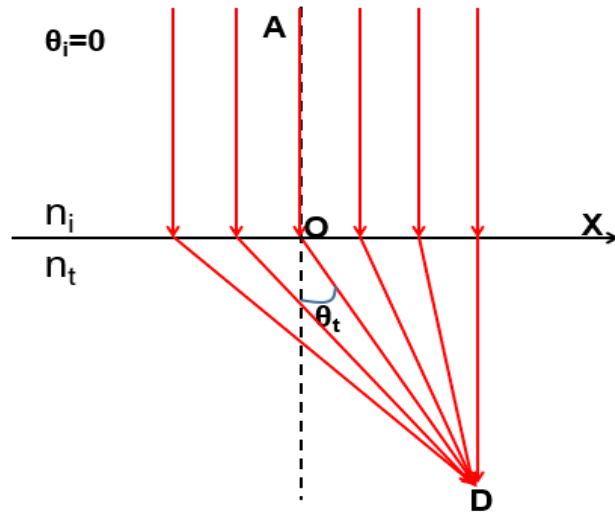


Fig. 2.11 Design of Metalens by Generalized Snell's Law

there any relationship between this design and the design of metalens we discussed last chapter?

To answer these questions, we want to compare equation 2.3.6 and equation 2.2.7, trying to find if there are some connection between them.

For equation 2.3.6, the Φ in this equation is defined as the phase discontinuity given by the interface (Phase difference between $\varphi(D)$ and $\varphi(B)$). As shown in Fig 2.12, $\sin \angle \theta_t =$

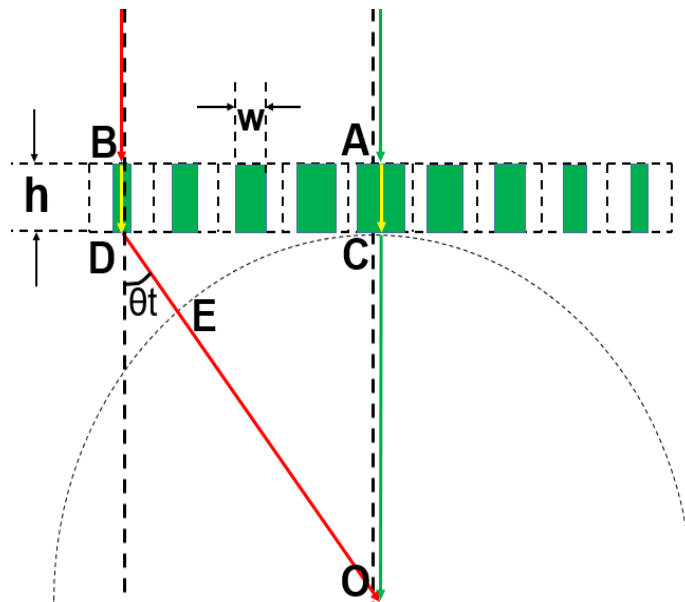


Fig. 2.12 Design of Metalens

$CD/OD = X/\sqrt{f^2 + X^2}$ and n_t equals one. So, we can simplify equation 2.3.6 to equation

2.3.7 (In this equation $\Phi = \varphi(B) - \varphi(D)$):

$$X/\sqrt{f^2 + X^2} = (1/k_0) \times (d\Phi/dx) \quad (2.3.7)$$

For equation 2.2.7, it seems a little bit similar to equation 2.3.7, but $\varphi(C)$ doesn't equal $\varphi(B)$. So, we assume that $\varphi(C)$ equals $\varphi(A)$, which means there is no phase shift at the center of lens. In this case, since the source provide a plane wave which means that $\varphi(B)$ equals $\varphi(A)$, we can prove that $\varphi(C)$ equals $\varphi(B)$. In this condition, we can change the form of equation 2.2.7 to 2.3.8 like this:

$$\varphi(D) - \varphi(B) = 2\pi \frac{\sqrt{f^2 + X^2} - f}{\lambda} \quad (2.3.8)$$

Then we make differential operations on both sides of the equation. One important thing needs to be mention here is that the direction of X in equation 2.3.8 is from right to left which is the negative direction in the derivation of Generalized Snell's Law. So, there should be a negative sign before dx when we do differential operation for the left part of equation 2.3.8. After several steps of simplification, equation 2.3.8 can be transferred to 2.3.9:

$$\begin{aligned} d(\varphi(D) - \varphi(B))/(-dx) &= d(2\pi \frac{\sqrt{f^2 + X^2} - f}{\lambda})/(dx) \\ d(-\Phi)/(-dx) &= d(2\pi \frac{\sqrt{f^2 + X^2} - f}{\lambda})/(dx) \\ d\Phi/dx &= \frac{2\pi X}{\lambda} / (\sqrt{f^2 + X^2}) \quad (2.3.9) \end{aligned}$$

Obviously, equation 2.3.9 is the same as equation 2.3.7 which demonstrates that we can utilize the method described in equation 2.2.7 in chapter 2.2 to realize a certain interface required by equation 2.3.6 which is expanded from Generalized Snell's Law in a certain condition that no phase shift at the center of lens ($\varphi(A)$ equals $\varphi(C)$). Up till now, we finished the derivation from equation 2.2.7 to equation 2.3.6, proving that they describe the same mechanism.

In conclusion, Generalized Snell's Law provides a new concept called phase gradient to help us understanding Metalens; and we can utilize the phase-mechanism method described in equation 2.2.7 in chapter 2.2 to design phase shifter arrays to achieve the certain phase gradient required by Generalized Snell's Law.

Chapter III Two-Dimensional & Three-Dimensional Metalens

3.1 Explanation and Steps of Metalens Design

1. Position vs Phase difference: According to the study in chapter 2.2, we figure out equation 2.2.7 which illustrates the relationship between the position of phase shifter and the phase difference (the difference between the phase of wavefront at point D and the phase of wavefront at point C).

2. Phase difference vs Phase shift: But what is the relationship between the phase shift given by the shifter at point D and the phase difference (the difference between the phase of

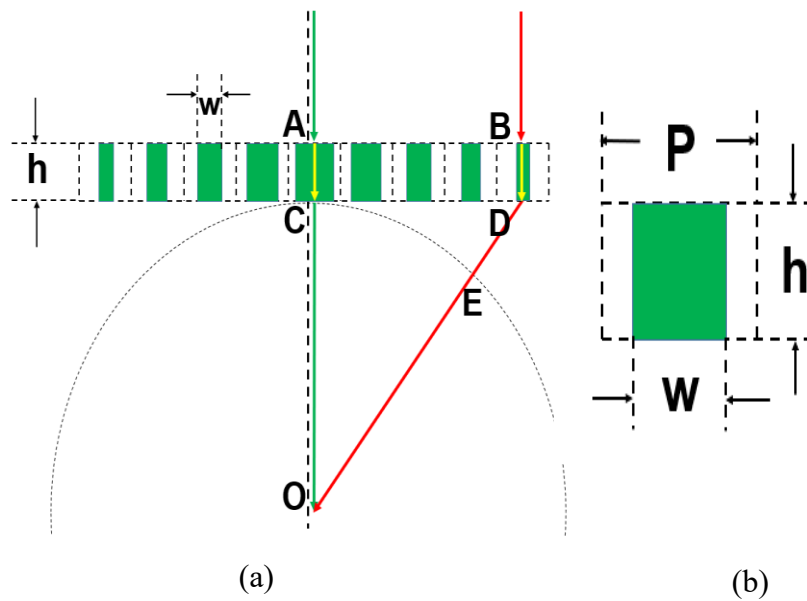


Fig. 3.1 Schematic of Metalens and Phase Shifter

wavefront at point D and the phase of wavefront at point C)?

In the certain condition that $\varphi(A)$ equals $\varphi(C)$, the phase difference has a same value as the phase shift. After several steps of transfer from equation 2.2.7, we can achieve equation 3.1.1:

$$\text{Phase difference} = \varphi(D) - \varphi(C) = 2\pi \frac{\sqrt{f^2 + X^2} - f}{\lambda} \quad (2.2.7)$$

$$(\varphi(D) - \varphi(B)) - (\varphi(C) - \varphi(B)) = 2\pi \frac{\sqrt{f^2 + X^2} - f}{\lambda}$$

$$(\varphi(D) - \varphi(B)) - (\varphi(C) - \varphi(A)) = 2\pi \frac{\sqrt{f^2 + X^2} - f}{\lambda}$$

$$\text{Phase Shift} = \varphi(D) - \varphi(B) = 2\pi \frac{\sqrt{f^2 + X^2} - f}{\lambda} \quad (3.1.1)$$

This equation gives the required value of phase shift needed to be achieved by the phase shifters at certain location. Up till now, we can just focus on the property of each phase shifters at their certain position, and the value of phase shift provided by each phase shifter is given by equation 3.1.1. After we figure out the value of required phase shift, we want to figure out how to realize the phase shift at the interface?

3. Phase shift vs W: In chapter 2.2, we have proposed a method to build phase shifters with different effective refractive index achieved by switching the W (width) of these phase shifters. Then we can use these phase shifters to obtain the appropriate phase shift at each position of the lens. So how can we figure out the exact value of W which provides the required phase shift at certain position?

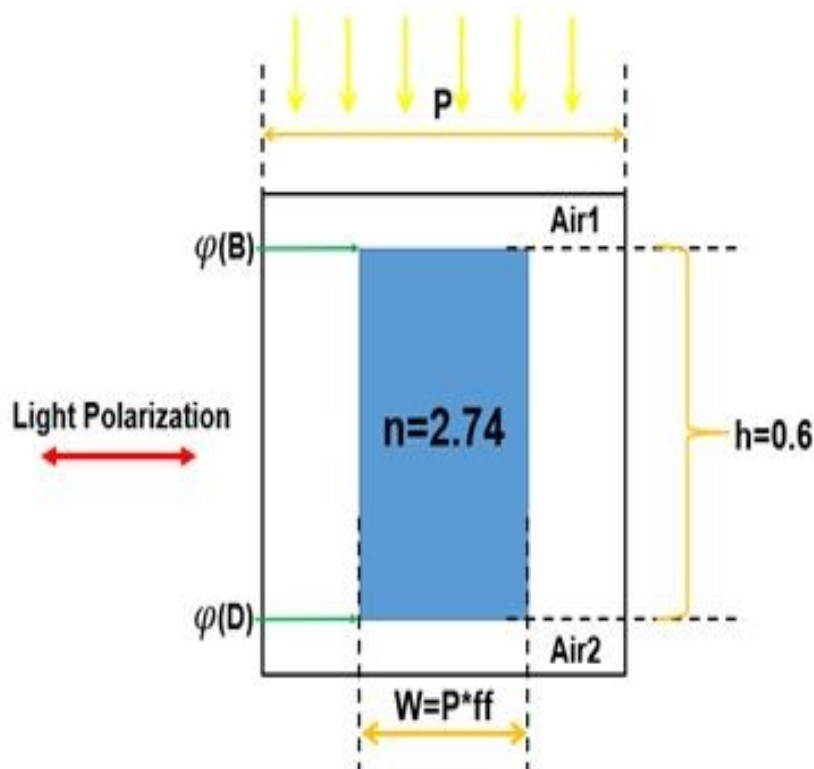


Fig. 3.2 Schematic of RCWA Simulation

Here, we utilize a simulation method called RCWA to test the phase shift. RCWA (Rigorous Coupled-Wave Analysis) engine is a function in OMNISIM to simulate periodic structure. As shown in Fig 3.2, it is one period of this periodic structure; and each period are the same. The dimensions of the Device along horizontal direction define the grating period as the structure is assumed to extend periodically and infinitely along the horizontal direction. The light source is a plane wave of 685nm at the top of this structure and the direction of the incident beam is perpendicular to horizontal direction. In Fig 3.2, P is period, W is the width of phase shifter ($W=P \times ff$), ff is fill factor, h is the thickness of the phase shifter. We record the phase of wavefront ($\varphi(B)$ and $\varphi(D)$) at each value of W during the simulation, and then we can get the value of phase shift by doing subtraction of $\varphi(B)$ and $\varphi(D)$, figuring out the relationship between W and Phase shift.

In order to find a better value of period, we write a program with two for loops, the variables are ff and P respectively ($h=0.6$, $n=2.74$). After that we can find an appropriate value of P which provides larger phase coverage. Then we extract the data of W and Phase shift at such value of P and import the data to Matlab to figure out the relationship between W and Phase shift (illustrated by an equation in Matlab).

4. Position vs W: In conclusion, equation 3.1.1 illustrated the Phase shift we need to achieve at certain location, then we utilize RCWA to figure out the value of W which can provide that Phase shift at that location. Finally, we combine them together and figure out the relationship between W and Position (X). This is the whole story of the design of metalens.

3.2 Simulation and Analysis of Two-Dimensional Lens

According to previous study, the design of metalens follows a widely acknowledged phase matching process. Basically, the metalens is consisting of a group of phase shifters that each of them will tune the phase of light based on its location. As mentioned previously, we have given an assumption that the phase shift at the center of lens is zero. The first reason for designing lens in this condition is the convenience in calculation that the value of Phase shift is the same as the value of Phase difference. In addition, this assumption helps us roughly determine the value of refractive index after we determined the wavelength of incident light.

We conducted this study through two-dimensional finite different (FDTD) time domain method under light incidence of 685nm. To achieve larger phase coverage, we need to increase the thickness of phase shifters. Since it is difficult to fabricate structures with high aspect ratio (e.g. Usually higher than 5:1 thickness vs. width), we thought about high

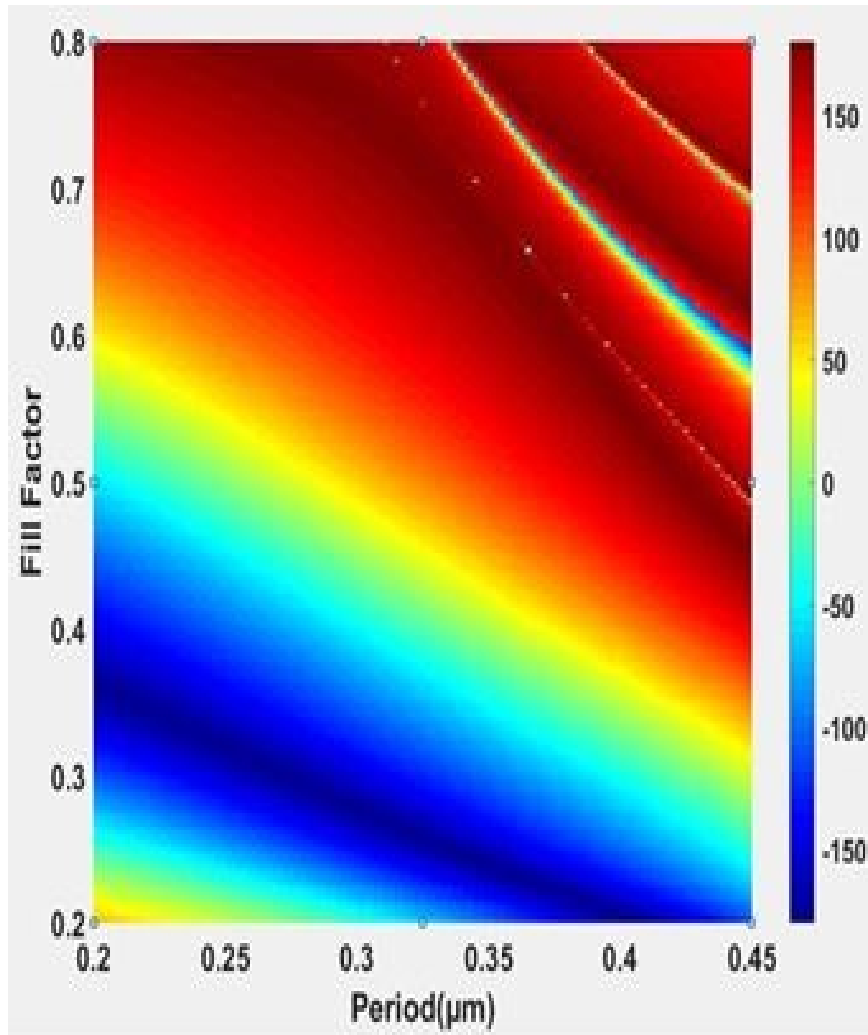
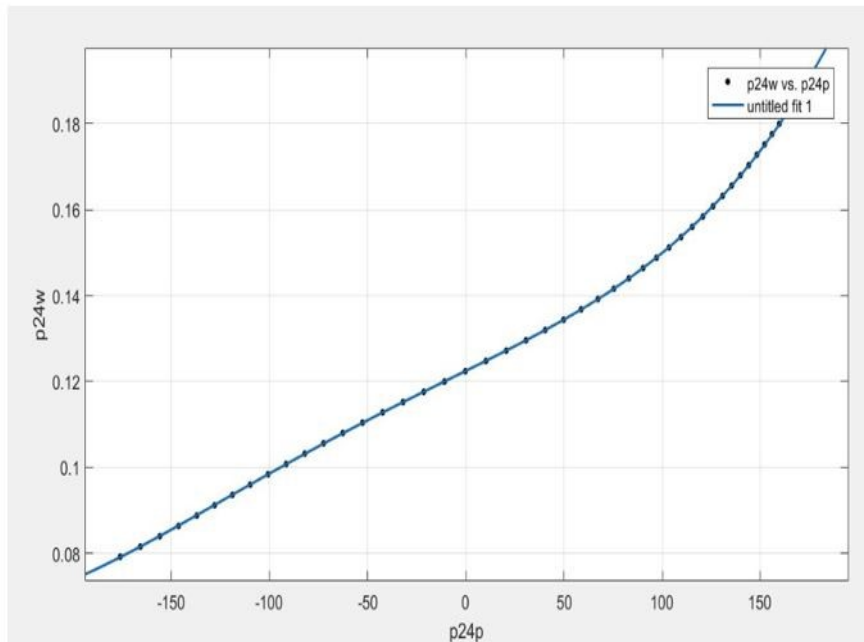


Fig. 3.3 Phase diagram for Si₃N₄ phase shifter

refractive index material such as Silicon rich Silicon nitride (refractive index 2.74). Shown in Fig 3.3 for a single Si₃N₄ phase shifter with thickness of 600 nm, the phase can be shifted in a range of 360 degrees (2π) with the variation of nano structure dimensions (period from 0.2 to 0.45 μm, fill factor from 0.2 to 0.8). Then we can select some better values of period and import the data of fill factor and phase shift to Matlab to achieve the relationship between them. E.g. Period as 0.24 μm, we can achieve the relationship between W and Phase shift

shown in Fig 3.4(a). According to observe how fit the curve is, we can figure out the order of the function we need. Utilizing equation 3.1.1 and the function shown in Fig 3.4(b), we can



(a)

Linear model Poly4:
 $f(x) = p1*x^4 + p2*x^3 + p3*x^2 + p4*x + p5$
 Coefficients (with 95% confidence bounds):
 p1 = 1.134e-11 (1.105e-11, 1.164e-11)
 p2 = 2.985e-09 (2.958e-09, 3.012e-09)
 p3 = 6.329e-08 (5.448e-08, 7.21e-08)
 p4 = 0.0002269 (0.0002263, 0.0002275)
 p5 = 0.1225 (0.1224, 0.1225)

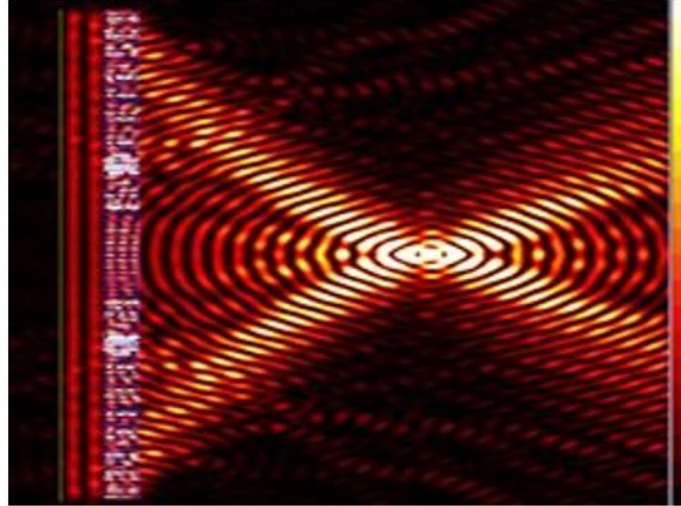
Goodness of fit:
 SSE: 2.847e-07
 R-square: 1
 Adjusted R-square: 1
 RMSE: 8.137e-05

(b)

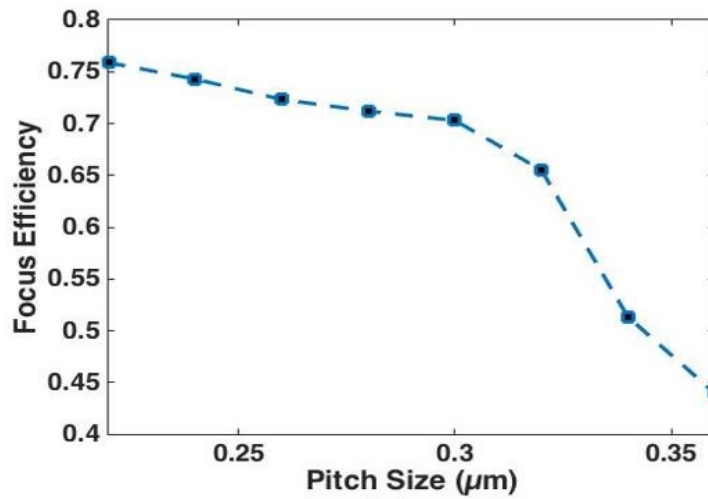
Fig. 3.4 Relationship between Phase shift and Width.

(a) Relationship illustrated by curve. (b) Relationship described by equation.

achieve the Matlab program to design our metalens (NA=0.9). As shown in Fig 3.5 (a), after the simulation step, we can achieve the field distribution and calculate the focus efficiency. In this study, we designed a series of metalens in 2-D with pitch size (period) ranging from 220



(a)



(b)

Fig. 3.5 (a) Field distribution of 2-D lens (Period=0.24, NA=0.9).
 (b) Focus efficiency of simulated metalens (NA=0.9) in 2-D with pitch size (period) ranging from 220 nm to 360 nm.

nm to 360 nm. These lenses are designed with high numerical aperture $NA = 0.9$. The thickness of the lens is fixed at 600 nm and the feature size is set around 50 nm. FDTD simulation is performed for all lenses under appropriate conditions (small enough grid size and long enough simulation time is applied). The size of the lens is fixed at 20 μm due to limited computing resources. And the focus efficiency is plotted in Fig. 3.5 (b). As shown in Fig. 3.5 (b), the focus efficiency increases from 44.8% to 75.8% with the decrease of period size from 360 nm to 220 nm. The field distribution of the lens designed with 220 nm period and 360 nm period

are shown in Fig 3.6(a) and (b) respectively. The background intensity is magnified at

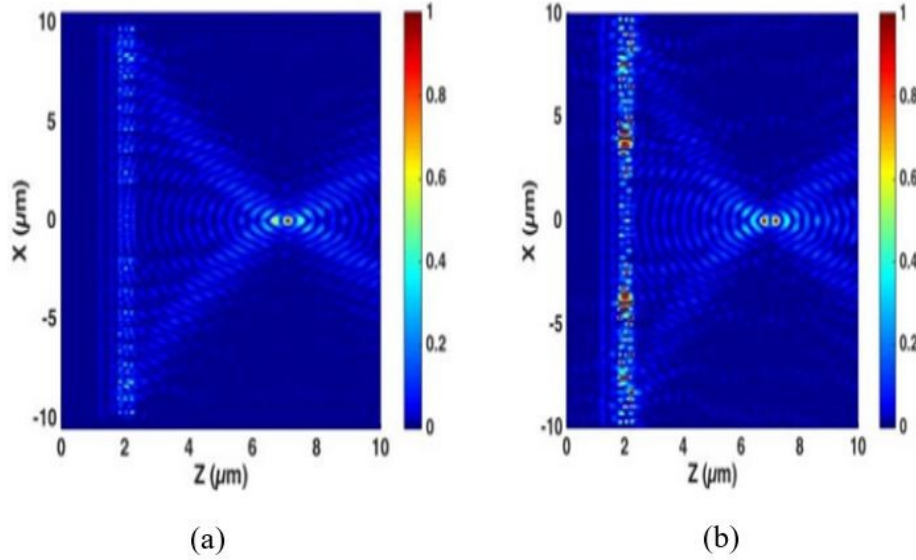


Fig. 3.6 (a) Field distribution of 2D metalens designed with 220 nm pitch size.
 (b) Field distribution of 2D metalens designed with 360 nm pitch size.

a same level in order to observe scattered light more clearly. As can be observed, Fig 3.6(a) shows a smooth concentrating profile which is in clear comparison with Fig 3.6(b). The lens designed with 360 nm pitch size shows strong resonance behavior at lens plane compared with 220 nm pitched lens. And the scattered light outside the focusing profile is notable in Fig 3.6(b). This decrease of focusing performance of 360 nm pitched lens (compared with 220 nm lens) is a result of coarse space discretization. In this case, scattering and undesired resonance become more significant. In conclusion, in order to achieve higher efficiency, we need to select smaller pitch size of phase shifter.

Furthermore, in the previous derivation of Generalized Snell's Law, we have assumed that Φ is a continuous function of the position along the interface; thus, all the incident energy is transferred into the anomalous refraction. However, because experimentally we use an array of phase shifters with subwavelength separation to achieve the phase change along the interface, this discreteness implies that there are also regularly refracted beams, which follow conventional laws of refraction, causing the decrease of efficiency. This explanation also proves that to increase the efficiency of metalens is to shrink the pitch size (period).

3.3 Design and Optical Characterization of Three-Dimensional Lens

The method to design 3D lens is quite similar to the mechanism of 2D lens. Since the phase shifters have the same thickness, we analyze the top view of lens to figure out the parameter of the phase shifters at different positions.

We have established a Cartesian coordinate system with X-axis and Y-axis. The center of the lens is defined at the origin of this coordinate system. The relationship between the phase shift and the location of phase shifter is described in equation 3.3.1:

$$\text{Phase Shift} = \varphi(D) - \varphi(B) = 2\pi \frac{\sqrt{f^2 + Y^2 + X^2} - f}{\lambda} \quad (3.3.1)$$

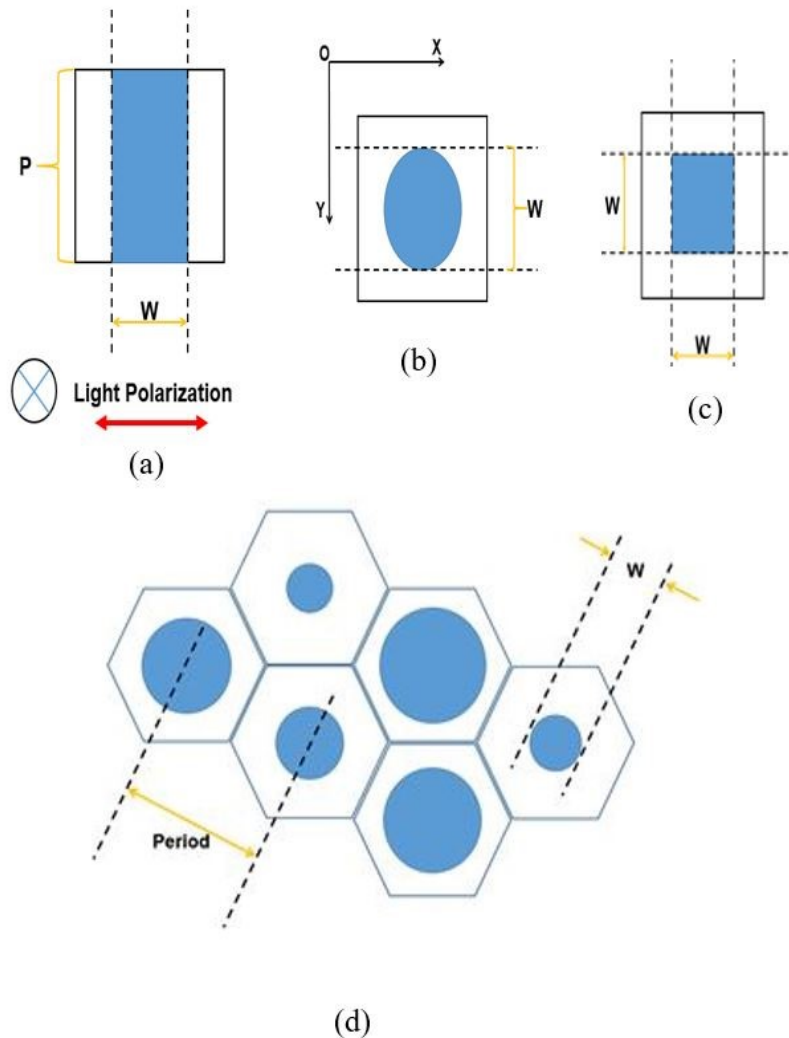


Fig. 3.7 Different kind of phase shifters.
 (a) Rectangular nano structure. (b) Ellipse nano structure.
 (c) Square nano structure. (d) Hexagon-array nano structure.

Different shapes of phase shifter (nano structure) can be used to complete the interface; and the shape of each period (lattice) of these phase shifters are often square or hexagon. As shown in Fig 3.7(a), it is a kind of phase shifter with rectangular nano structure and square lattice, just switching the value of W to achieve enough phase coverage to form a concentrating metalens. This kind of design can be utilized to linear distinguishing lens which we will discuss in next chapter. The direction of the incident light is perpendicular to this

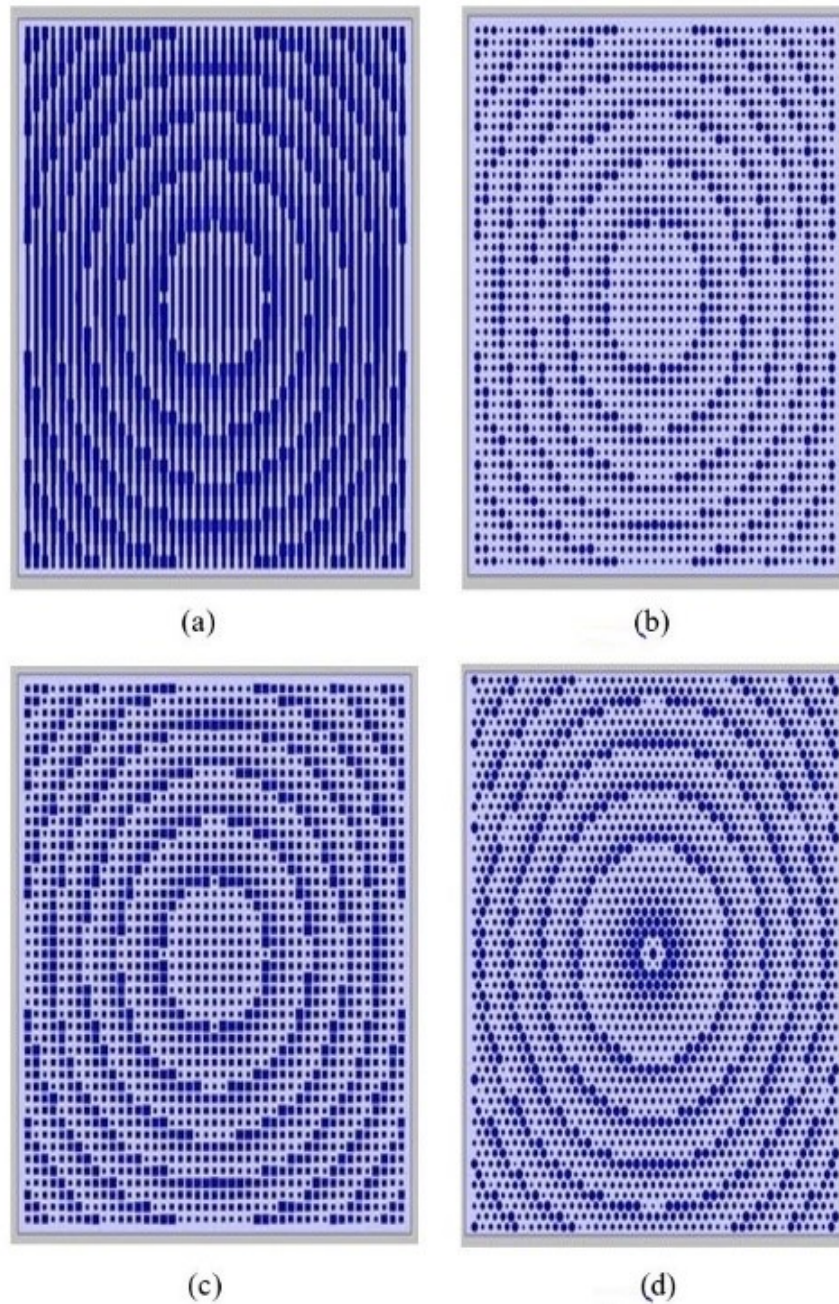


Fig. 3.8 Design of Metalens ($10\ \mu\text{m}\times 10\ \mu\text{m}$)

paper and the light is polarized as shown in Fig 3.7(a). The Fig 3.7(b) illustrated an ellipse nano structure; and the lens made by this structure specializes in focusing circular polarized light. For square period (lattice), we can also utilize square nano structure with different side length to compose the metalens as shown in Fig 3.7(c). The metasurface can also be composed by an array of amorphous silicon nanoposts with different diameters that are arranged in a hexagonal lattice as shown in Fig 3.7(d). Here, we define that the distance between each center is period and the diameter of the nanoposts is W . No matter which kind of lattice we select, the periodic graphics (lattice) must fill all the plane, just like laying bricks on the ground. Although different kinds of phase shifters correspond to different kind of incident light and need to be fabricated by different kind of methods, the focus mechanism shown in equation 3.3.1 works to all of them. Fig 3.8 shows a series of metalens designed in 3-D, composed by four different kinds of phase shifters respectively as we mentioned before.

Up till now, we have proposed four kinds of three-dimensional lens, and the final structure we would mention is called grating lens. Different from other four structures, a grating based metalens is designed by rotating the 2-D phase profile along its central axis with its diameter. As shown in Fig 3.9, it is a grating metalens with $NA=0.9$ and diameter

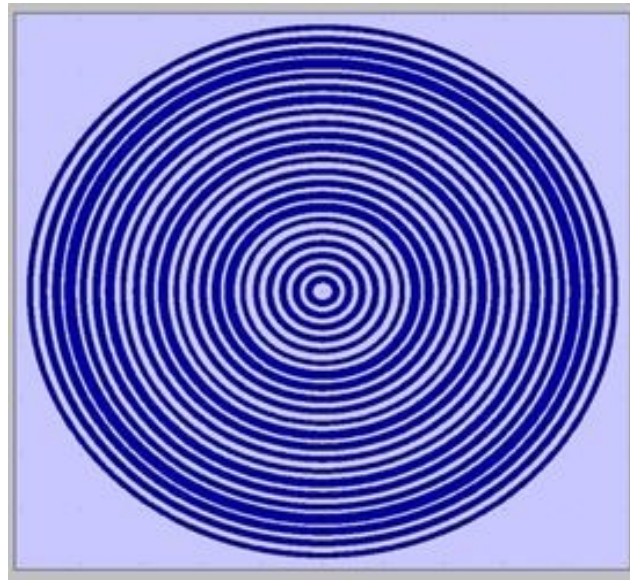


Fig. 3.9 Design of Grating lens ($10\ \mu\text{m}\times 10\ \mu\text{m}$)

of $10\ \mu\text{m}$ at the wavelength of $685\ \text{nm}$. Since its special symmetrical composition, grating lens is able to provide the same focus efficiency for incident light polarized in any direction.

By the way, the fabrication of grating lens is very different with those four mentioned previously.

After the design, we performed FDTD simulation for all lenses under appropriate

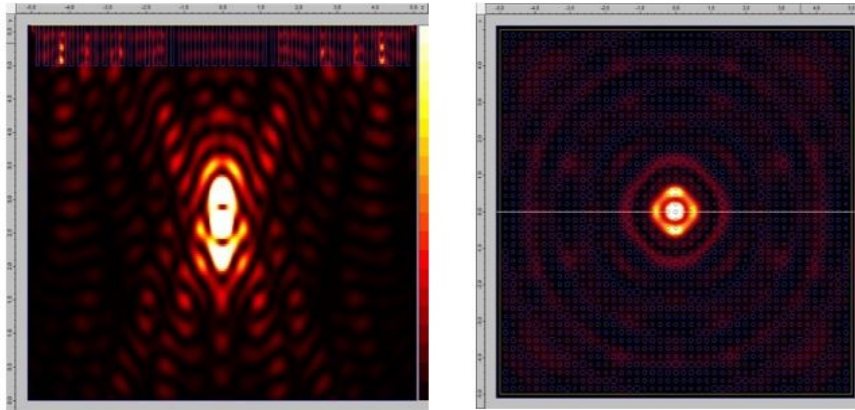


Fig. 3.10 Field distribution of 3D simulation

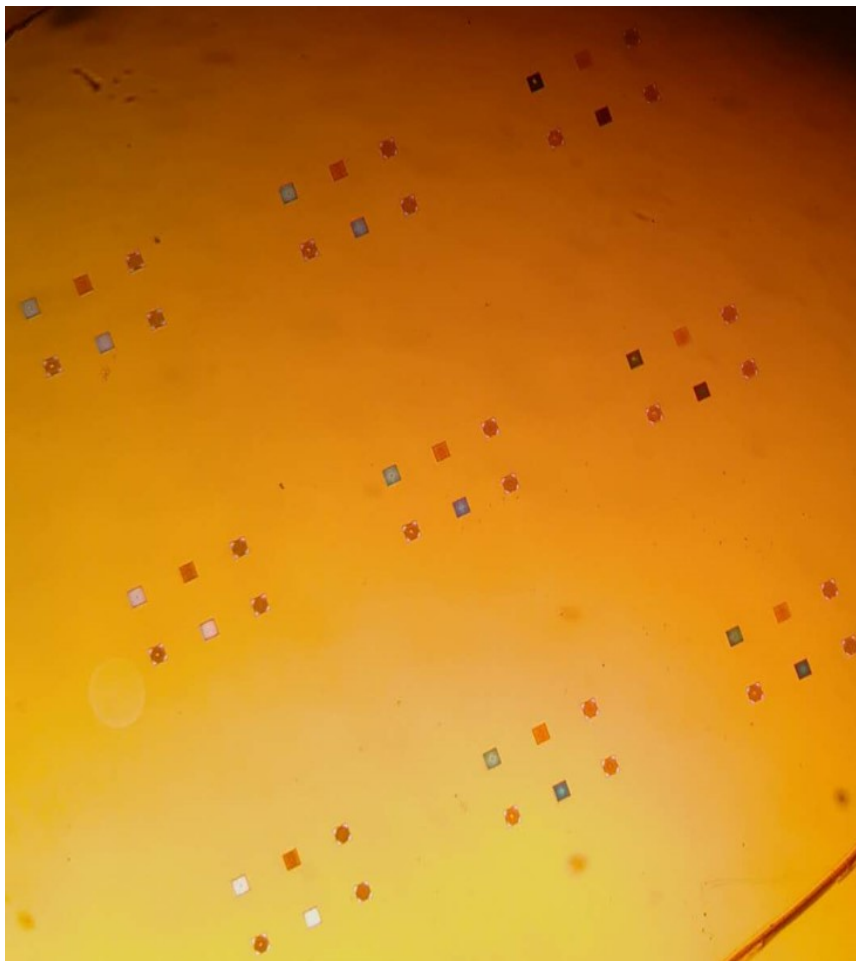
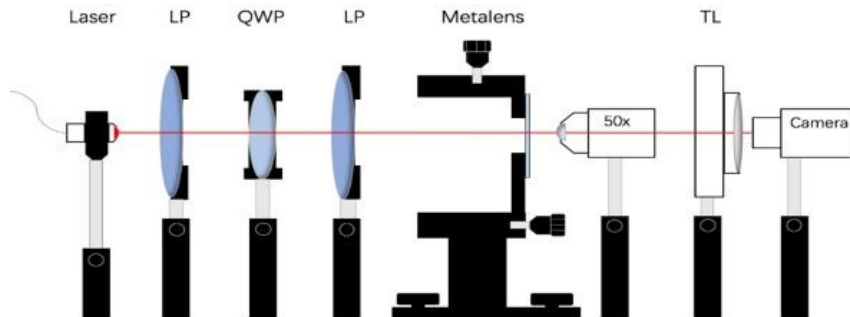
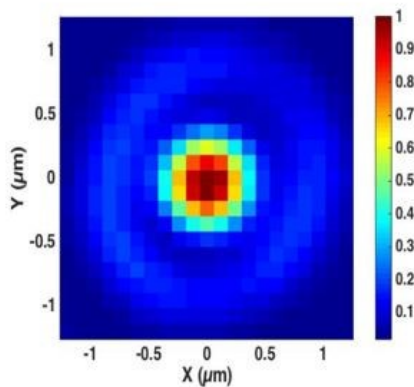


Fig. 3.11 Nine groups of lenses, each group with six kinds

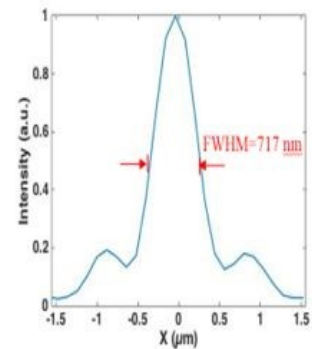
condition (small enough grid size at 37 nm and long enough simulation time is applied). The size of lens is fixed as $10\ \mu\text{m} \times 10\ \mu\text{m}$ due to limited computing resource. And the field distribution of one lens composed by ellipse nano structure with 220 nm period is plot in Fig



(a)



(b)



(c)

NA	Focus Efficiency
0.99(Grating)	1.3%
0.90(Grating)	3.4%
0.90(Cylinder)	4.9%
0.90(Polarization)	3.8%
0.50(Grating)	36%
0.50(Cylinder)	39.9%

(d)

Fig. 3.12 Optical Characterization

3.10. The focus efficiency of these lens with high numerical aperture $\text{NA}=0.9$ can reach 55%.

Due to the limited computing resource, at most we are able to perform the simulation of a 3-D lens with size $15\ \mu\text{m} \times 15\ \mu\text{m}$. But we can fabricate lenses with larger size. In this case, we utilized OMNISIM to design lenses with size $40\ \mu\text{m} \times 40\ \mu\text{m}$ and layout the schematics of

our design to make fabrication. In this study, we had fabricated six kinds of lenses: (A) Cylinder NA=0.5, (B) Polarization dependent NA=0.9, (C) Grating NA=0.99, (D) Grating NA=0.5, (E) Cylinder NA=0.9, (F) Grating NA=0.9. As shown in Fig 3.11, in our last sample we have 9 groups of lenses with different lithography parameters, we have improved our technique to get detailed specs of lens for several groups.

The optical characterization system for our lenses is shown in Fig 3.12(a). A diode laser of 685 nm (LP685-SF15, Thorlabs) is applied as light source. This optical system also includes quarter waveplate, linear polarizer, 3-axis motion mount, 50x objective, tube lens and camera.

The characterized field distribution of grating lens (NA=0.5) on the plane of focus is shown in Fig 3.12(b) and the focus profile is plot in Fig 3.12(c). The measured focus efficiency is around 36% with diffraction limited FWHM of 717 nm. By the way, the efficiency of all the kinds of lenses are shown in Fig 3.12(d).

It seems that the larger the NA, the weaker the focus efficiency. While 3-D FDTD simulation of this lens indicating a much higher focus efficiency of 55%. In addition, Fig.

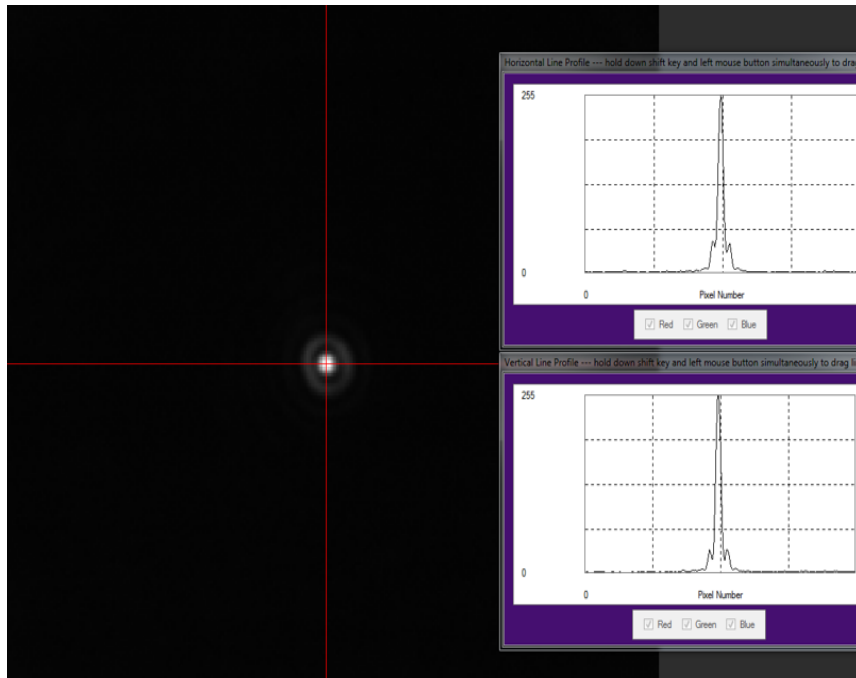


Fig. 3.13 Focus image received by camera

3.13 shows the image of the focus of grating lens at NA=0.90 received by the camera, and this property is very good. Even an airy disk can be observed from the image which is

indicating good focus behavior. So, we think this difference of focus efficiency between simulation and characterization is mainly caused by the limitation of characterization system in two aspects: 1. The 50x objective applied (Olympus, LMPLFLN 50x) has NA of 0.5 which is considerably lower than our lens's NA =0.9 and NA=0.99. As a result, it is not able to catch the peak intensity of diffraction limited focus, since the size of focus become extremely small when the NA is near unity. In this case, we can explain that why the efficiency of the lenses at NA=0.5 is much higher than NA=0.9 or NA=0.99. 2. The resolution for motion system (Thorlabs, MT3A) is 0.5 μm , which is similar to the size of diffraction limited focus (532 nm). In this case, the capture of exact focal plane become extremely challenging.

Chapter IV Linear Polarization Distinguishing Metalens in Visible

Leading-edge research about metalens has raised wide interest due to its planar structure and unprecedented control of light through subwavelength nano structures. In this study, we propose a novel metalens that integrates the function of concentrating lens and linear polarizer. For this lens, focus can only be formed under the incidence of designed linear polarization while its focusing effect is significantly suppressed with the incidence of its orthogonal linear polarization. The performance of this lens is verified by both simulation and characterization. The linear distinguishing property is rooted from the special design of anisotropic subwavelength phase shifters with polarization-selective effective index while generating scattering loss on the incidence of unwanted polarization at the same time. This study paves the way for the development and integration of multiple functionalities on emerging metasurface while opening another door for the replacing of traditional bulk optical component with planar and compact metasurface.

4.1 Introduction of Polarization

Traditional control of polarization is basically achieved through optical devices namely, polarizer and wave plate. Linear polarizer allows the propagation of certain linearly polarized electro-magnetic wave while prohibits its orthogonal polarization by either absorption or redirection (through birefringent effect). Wave plates are typical application of a number of birefringent materials that upon propagation, a designed phase difference is created between orthogonal optical axis, which changes the polarization state of the propagated electro-magnetic wave. With the development of metasurface, researchers are able to create subwavelength birefringence unit in nano scale. This has led to the design and fabrication of metalens utilizing Pancharatnam-Berry phase (also known as geometric phase) based on circularly polarized incidence. The basic structures (phase shifters) of these metalens are (in most cases) a group of cuboids with space-variant orientation. These phase shifters can also

be considered as small waveplates. By tuning the orientation of these tinny waveplates, researchers are able to acquire 2π phase shift coverage which is essential for lens design. In addition, it is possible to distinguish circular polarization state (e.g. left-handed circular polarization, LCP and right-handed circular polarization, RCP) by applying two sets of phase shifters in one lens, which results in a hybrid metalens that creates different focus or image with the incidence of LCP or RCP light. Even though linearly polarized light can be viewed as the superposition of left-handed and right-handed circularly polarized light, it is not efficient to design the metalens for linearly polarized incidence with Pancharatnam-Berry phase shifters, because each phase shifter only works under certain polarization (e.g. either LCP or RCP). In order to achieve metalens for linearly polarized incidence, researchers have looked into the modification of propagation phase. This modification is usually achieved by altering the size of nano structure (e.g. period and fill factor) at sub-wavelength scale that the phase shifted (e.g. phase shift of the 0th diffraction mode) upon propagation is altered. With the help of modern computer aided calculation tool (e.g. FDTD and RCWA), people are able to acquire the phase shift for a number of nano structures with various of dimensions and materials. The metalens for linear polarized incidence is then formed by a group of nano structures with space-variant dimensions. These phase shifters are usually appeared as cylinders with space-variant diameters and are considered as polarization-intensitive.

In this study, we designed, fabricated and characterized a linear polarization distinguishing metalens by increasing the polarization sensitivity of individual phase shifters, while maintaining necessary phase coverage on the designed polarization. The linear polarization distinguishing performance of this metalens is confirmed by both simulation and optical characterization. This is the first focusing metalens designed with linear polarization distinguishing effect.

4.2 Design Strategy of Linear Polarization Distinguishing Metalens

For metalens designed under linear polarized incidence, the control of phase is achieved by the variation of nano structure at the lens plane (e.g. the variation of period and fill factor). At 3-D domain, conventional phase shifters for concentrating metalens are mostly cylinder nano structures confined within individual period shaped by square (Fig. 4.1 a) or hexagon.

In other words, their 2-D lens plane is discretized into finite number of squares or hexagons. In this case, the phase variation is achieved by tuning the diameter of cylinder nano structure, so the effective index is varied within the period. While this design is polarization-intensitive, because for each phase shifter, the variation of effective index with the change of incident polarization is negligible. Another example of polarization intensitive metalens is the grating metalens. By rotating the 2-D design (e.g. Fig 4.1 c, cross-section at $x = 0$) along the central axis, metalens can be designed with concentric rings structure and this design is purely isotropic.

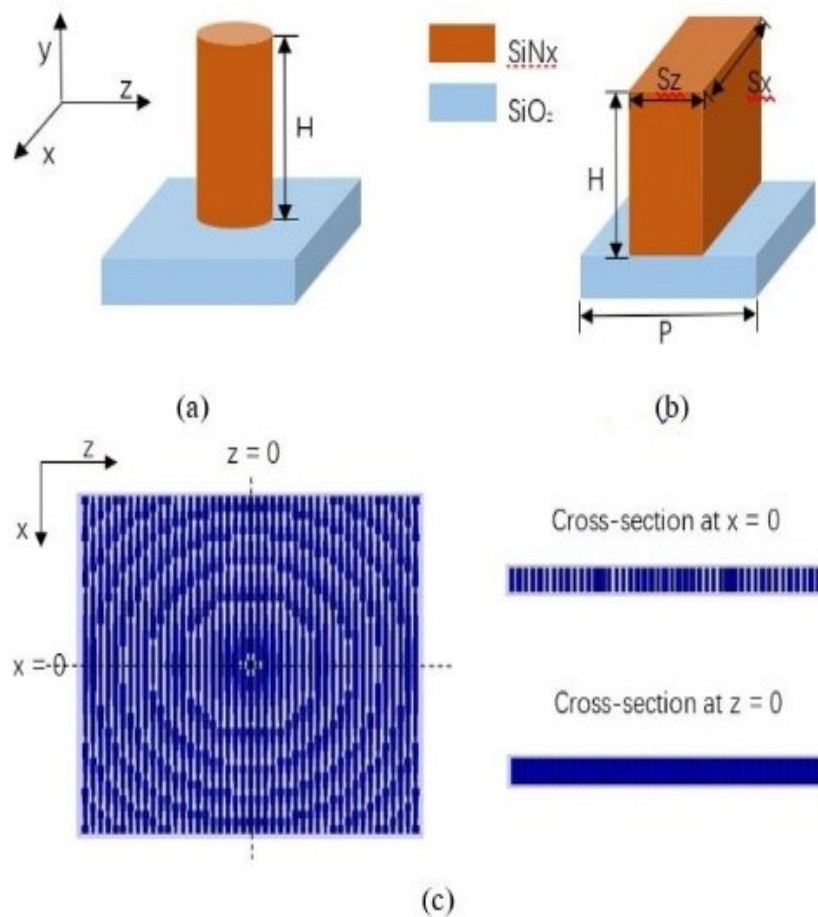


Fig. 4.1 (a) Structure of traditional phase shifter for linear polarized incidence. (b) Structure of linear polarization distinguishing phase shifter. (c) Design layout of polarization distinguishing metalens

In order to achieve linear polarization distinguishing effect, we have designed a novel phase shifter that is highly sensitive to the variation of linear polarization. The 3-D structure for this phase shifter is shown in Fig 4.1 (b). The lens plane is discretized into infinite number

of squares (e.g. the shape of period is square) with period P . The size of period has to be small enough compared to the incident wavelength in order to avoid diffraction loss (e.g. $P < \lambda/2NA$). The thickness H is fixed at 600 nm for all phase shifters. The thickness of phase shifter is critical for metalens designed under linear polarized incidence as the phase utilized is propagation phase (different from Pancharatnam-Berry phase), sufficient H is necessary to achieve 2π coverage. The size along x axis (e.g. S_x) is equal to P , which indicating that the

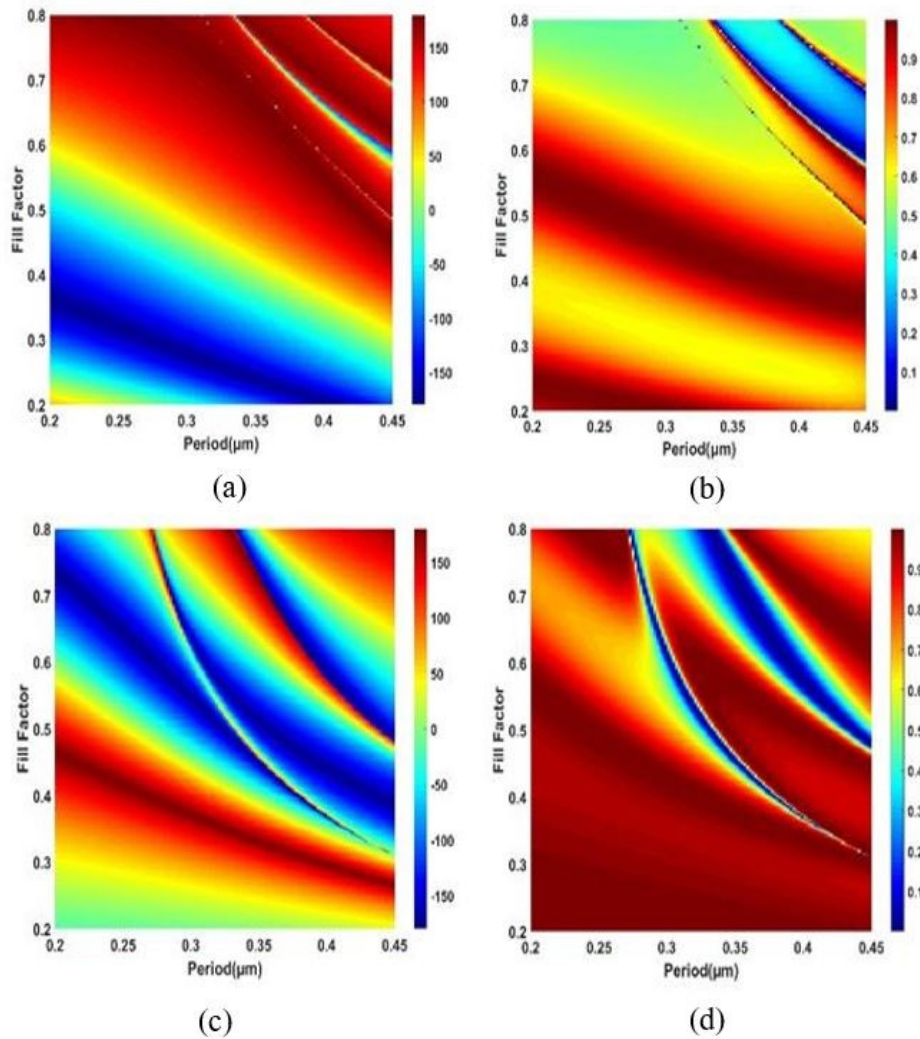


Fig. 4.2 Phase and Transmission Diagram for linear polarization distinguishing phase shifters. (a) Phase diagram for E_z incidence. (b) Transmission for E_z incidence. (c) Phase diagram for H_z incidence. (d) Transmission for H_z incidence.

period is fully filled in x direction with high index lens material. By this approach, we physically reduced the variation of effective index in X direction. The size along Z axis (e.g.

S_z) is varied to acquire the phase shift needed by equation (3.3.1) under E_z polarization. The lens material utilized here is silicon rich silicon nitride (SiN_x in Fig 4.1) with refractive index $n = 2.74$, extinction coefficient $k = 0$ at the design wavelength of 685 nm. The reason for the utilization of high refractive index SiN_x as lens material is also rooted from the need of sufficient propagation phase shift within small period. The lens is designed on glass wafer with $n = 1.46$ and thickness of 500 μm . The optical properties of glass wafer and SiN_x films are measured through woollam M-2000 ellipsometer. By matching the phase requirement in equation (3.3.1), a polarization distinguishing lens is designed and shown in Fig 4.1 (c) with top view and cross section views (light is incident in Y direction).

The phase and transmission map for the polarization distinguishing phase shifter is shown in Fig 4.2, where the fill factor is the fraction of period that is filled by the lens material ($S_z = \text{Period} \times \text{Fill Factor}$). This phase and transmission map is calculated through rigorous coupled wave analysis (RCWA, Photon Design Ltd.). The design polarization is E_z with wavelength 685 nm. Since the numerical aperture for the lens is $\text{NA} = 0.9$, the largest period available is calculated as $P < \lambda / 2\text{NA} = 380$ nm based on conventional understandings mentioned previously. While as can be observed from Fig 4.2 (a), from period 0.3-0.38 μm , a continuous variation of phase shift is not accompanied with the constant change of fill factor, which is indicating the existence of scattering loss. To be specific, each individual period that forms metalens/metasurface is mimicking a homogenous medium with different effective index. In this case, the effective index is tuned by the fill factor, so ideally, the phase shifted is supposed to be in positive correlation with fill factor. Otherwise there may be scattering or unwanted resonance. As a result, the upper limit for period is redefined to 0.3 μm .

In order to achieve linear polarization distinguishing effect, other than enhancing the focus under E_z polarization, it is also important to reduce its performance under H_z . This can be achieved through two approaches. The first one is to reduce the phase coverage under the incidence of H_z while maintain 2π coverage under E_z . As calculated from Fig 4.2 (a) and (c), at $0.22 < P < 0.3$ μm , there exists 2π phase coverage (e.g. when fill factor is varied) under E_z . While its phase covered under H_z varies from 1.2π to 1.33π , which does not show significant improvement. The other approach is to create scattering loss at unwanted incident

polarization. As aforementioned, each period inside metalens/metasurface is mimicking a homogeneous medium with effective index tuned by fill factor. Failure of continuous tuning of phase shift by constant change of fill factor is indicating strong scattering or unwanted resonance, which can be observed in Fig 4.2 (c) at $0.26 < P < 0.3 \mu\text{m}$ area (between dashed lines). This means phase shifters designed within this area experience strong scattering loss under Hz polarized incidence while remains stable tuning of phase under Ez polarized incidence, which is the property of our interest.

Even though smaller period generally indicating better lens performance, the lower limit of P is restricted by current nano fabrication technology as the fabrication of small nano

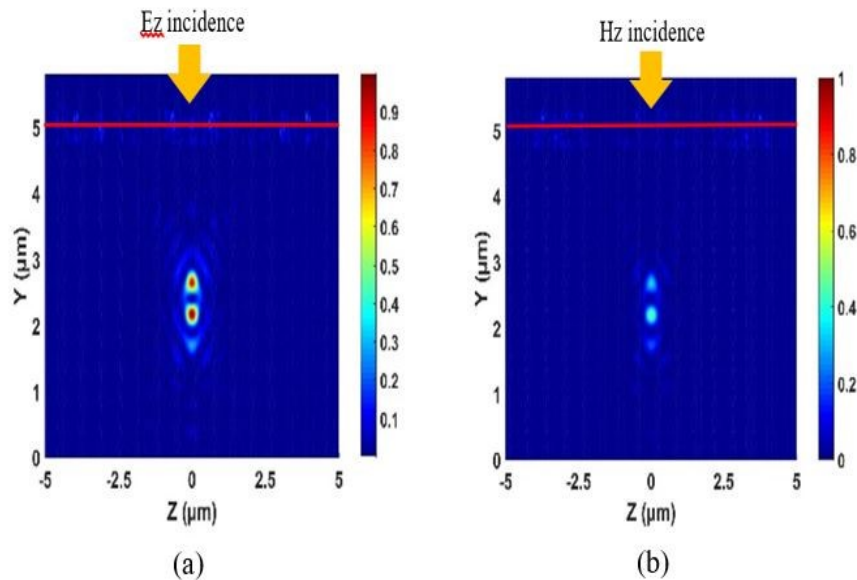


Fig. 4.3 Field distribution at cross-section $x=0$ of the lens at Ez and Hz incidence.

(a) Field distribution under incidence of Ez Polarization.

(b) Field distribution under incidence of Hz polarization.

structure with high aspect ratio is very challenging (in this case $H=600 \text{ nm}$) either by deep reactive ion etching (DRIE) or lift-off process. By considering the trade-off between performance and fabrication, we finally pick $P=280 \text{ nm}$ and designed a $10 \times 10 \mu\text{m}$ polarization distinguishing lens with numerical aperture $NA=0.9$ for the proof of concept simulation. The smallest feature in this lens is around 48 nm .

4.3 Simulation and Discussion

The performance of this lens is then simulated by 3-D finite difference time domain (FDTD) method (Omnisim, Photon Design Ltd.). Perfect match layer (PML) is applied on all boundaries of simulation window to truncate simulation space. Refractive index of SiO₂ substrate and air are 1.46 and 1 respectively. Imaginary part of refractive index for glass and air are set zero, sufficient small grid size and sufficient long simulation times are applied for the simulation.

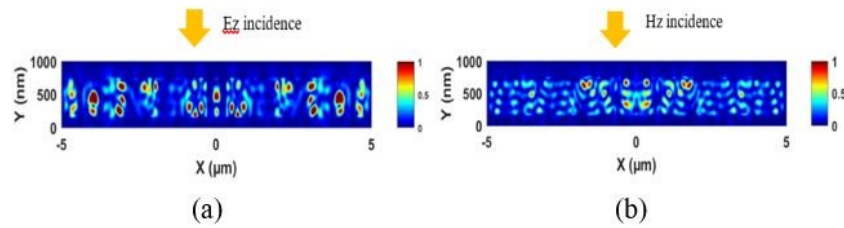


Fig. 4.4 Field distribution of lens. (a) Field distribution of lens when Ez is incident. (b) Field distribution of lens when Hz is incident.

The field distribution of the cross-section $x=0$ of the simulated field is shown in Fig 4.3. As can be observed in Fig 4.3 (a), a strong focus is formed at the designed focus spot with focal length around $2.5 \mu\text{m}$. This is in clear comparison with Fig 4.3 (b) where a focus can hardly be observed when incident is switched to Hz polarization. The focus efficiency is calculated by collecting the energy of $1.5 \times 1.5 \mu\text{m}$ area at the focal plane (e.g. $2.5 \mu\text{m}$ away from lens plane) divided by the $10 \times 10 \mu\text{m}$ energy collected at lens plane (without lens structure to avoid reflection). The focus efficiency is 48.9% for Ez incidence (comparable to state-of-the-art metalens under linear polarization with similar NA) and 14.5% for Hz incidence. The suppressed focus performance under Hz polarization is rooted from the anisotropic design of phase shifter and our aforementioned selection of period which generated the scattering loss under this polarization.

The field distribution inside lens is shown in Fig 4.4 with magnified picture of $x=0$ cross-section. As can be observed from Fig 4.4 (a), there exist strong resonance inside the lens. While the resonance become much weaker when Hz is incident (Fig 4.4 b). Because the excitation of focus mode/ resonance is critical for the formation of focus, this also explained the suppressed focus performance under incidence of Hz polarization.

4.4 Fabrication and Characterization

A polarization distinguishing lens with diameter of 40 μm and numerical aperture of 0.9 (NA=0.9) is then fabricated with CMOS compatible nano fabrication techniques. We start with 4-inch glass wafer as substrate with thickness of 500 μm . A silicon rich silicon nitride (SiNx) layer with thickness of 600 nm is deposited on the substrate as lens material. A silicon dioxide layer with thickness of 300 nm is then deposited on top of SiNx layer as a hard mask. Plasma enhanced chemical vapor deposition (PECVD) is applied for both depositions. A photoresist layer (ZEP520A) of 200 nm is then spin coated on top of SiO₂ layer for lithography. The 2-D lens pattern is written by E-beam lithography (JEOL, Inc.) and the pattern is created on the photoresist mask after development. The lens structure is then transferred into SiO₂ hard mask layer by reactive ion etching (R.I.E.) and the residual photoresist is stripped through plasma stripper (YES, Inc.). The pattern is then transferred

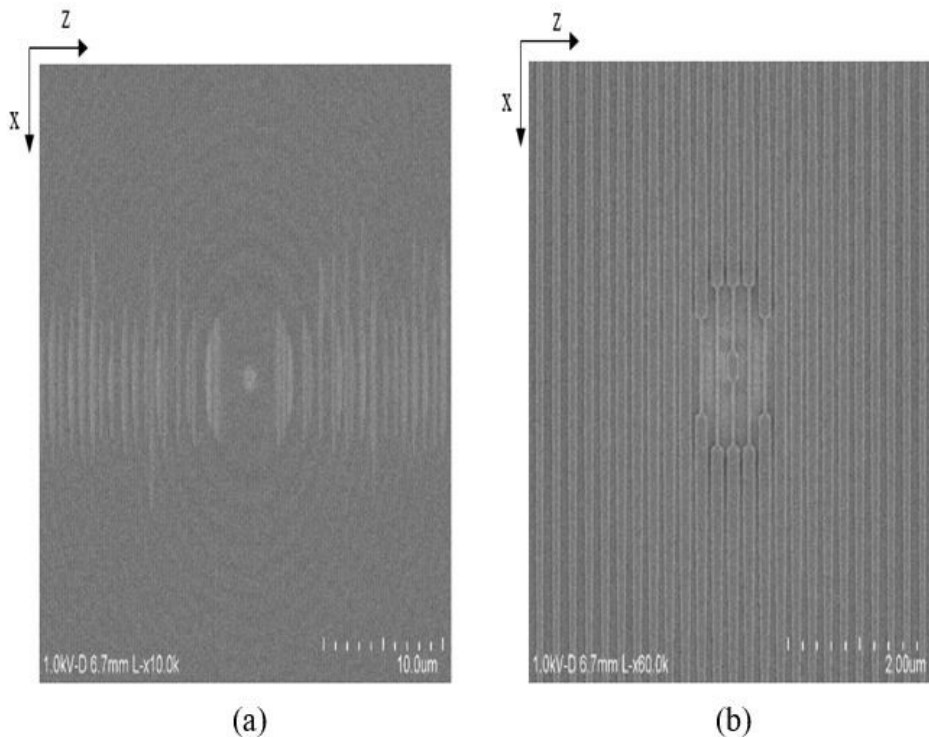


Fig. 4.5 SEM image of polarization distinguishing lens.
(a) Overall view of the lens (b) Magnified view at the center of lens.

into silicon rich nitride layer by another step of reactive ion etching and the remaining SiO₂ is removed by rinsing with hydro fluoric acid. The reason for our utilization of SiO₂ layer as hard mask is because there is no E-beam photoresist available (at 200 nm thickness) to provide enough selectivity versus SiN_x to achieve direct R.I.E. of 600 nm depth. While the thickness of E-beam resist is limited by our feature size of 48 nm. As a result, a two-step R.I.E. process with hard mask is necessary for the fabrication of this metalens.

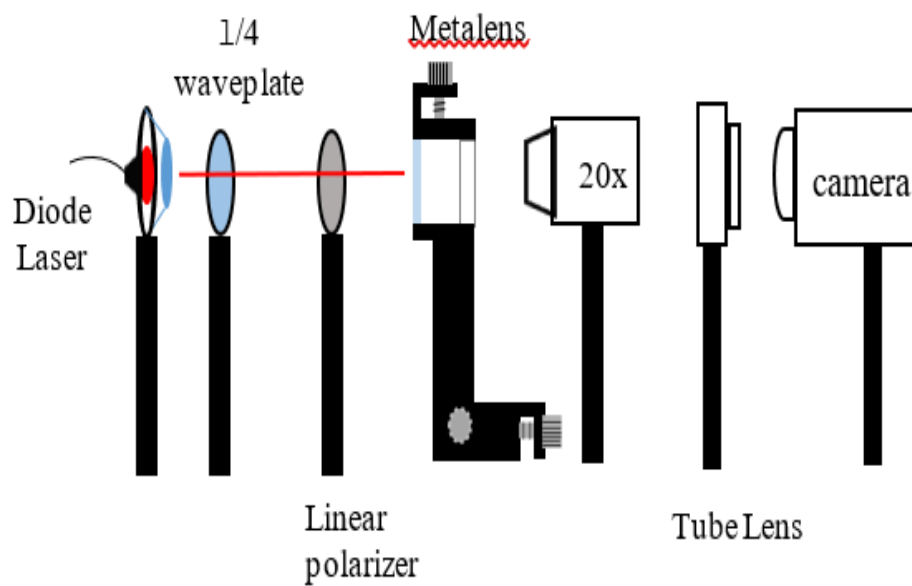


Fig. 4.6 Characterization system.

The SEM picture of the sample is taken after gold sputtering. The overall view is shown in Fig 4.5 (a), and the $5 \times 5 \mu\text{m}$ area at center of lens is shown in Fig 4.5 (b). The structure is physically formed by individual lines with width varied on x direction. The smallest feature is around 48 nm as measured.

The optical characterization system for this lens is shown in Fig. 4.6. A diode laser of 685 nm (LP685-SF15, Thorlabs) is applied as light source. Since the laser is linearly polarized, a quarter wave plate is applied to turn the light into circularly polarization. A linear polarizer is fixed on a rotation mount to achieve linear polarized light with tunable direction. The laser spot size on metalens is bigger than 1 cm which can be considered as plane wave when the center is collimated to our lens (the size of lens is $40 \mu\text{m}$). The image acquired is

magnified through a 20x objective lens and finally received by camera (DCC3240C, Thorlabs) through a tube lens. The sample is loaded on a 3-D axis motion system (MT3A, Thorlabs) with smallest trackable movement of $0.5\mu\text{m}$.

The characterized field distribution on the plane of focus is shown in Fig 4.7 (a) for the incidence of E_z and Fig 4.7 (b) for the incidence of H_z . It can be observed that a clear focus

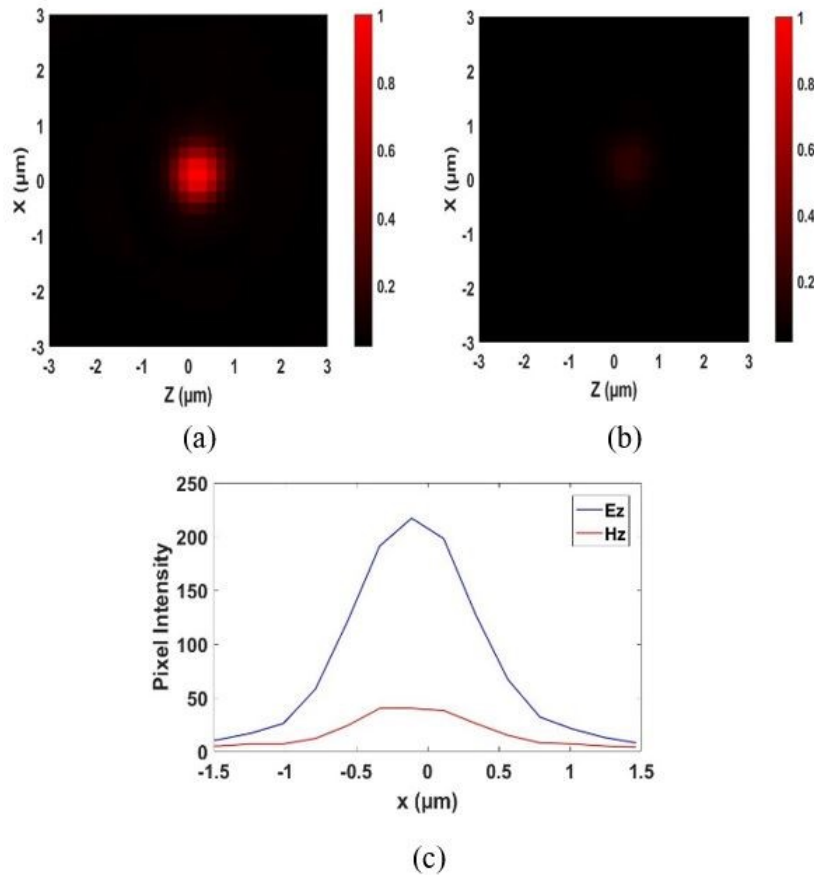


Fig. 4.7 Optical characterization of linear polarization distinguishing metalens under E_z (a) polarized incidence and H_z (b) polarized incidence. (c) Focus profile of both incident polarizations

is formed under the incidence of designed linear polarization E_z (Fig 4.7 a), and there is hardly any focusing effect when the incident polarization is tuned by 90 degrees (Fig 4.7 b). The focus profile is shown in Fig 4.7 (c). The peak intensity at designed polarization E_z is around 53 times of incident intensity with full-width-at-half-maximum (FWHM) of $0.9\mu\text{m}$. And the focusing behavior become much weaker for H_z incidence with around 7 times of incident intensity at peak and almost same FWHM with E_z .

4.5 Conclusion

In this study, for the first time a metalens is designed with the ability to distinguish linear polarization while maintaining concentrating performance comparable with the state-of-the-art metalens under linear polarized incidence. This design is achieved through the novel design of anisotropic phase shifter with scattering effect on unwanted polarization while maintain continuous phase shift on the orthogonal polarization. This study is a typical example of metalens integrating the function of two traditional bulk optical component: linear polarizer and concentrating lens. This study is especially attractive to applications including polarized light microscopy and optical communication where the orthogonal signal is focused and split.

With the inherent advantage of fully controlling the wavefront, metasurfaces promises a bright future for the integration of traditional optical components into compact and light weight thin films (metalens is usually as thin as several hundred nanometers). The major drawback of metalens is the difficulty and high cost of nano fabrication that holding it back from industrialization. But with the rapid development of nano fabrication technique which is also pushed by moore's law, mass production of metalens can be achieved in near future.

Chapter V Design and Simulation about 3D Metalens with Different Shapes of Focus

5.1 Straight-Line Focus

According to our design of 2-D lens, we know that the phase shifters along the vertical line in Fig 5.1 provide appropriate phase shift, making the incident light focusing at a certain point. In order to achieve a straight-line focus, we extend the length of these phase shifters in

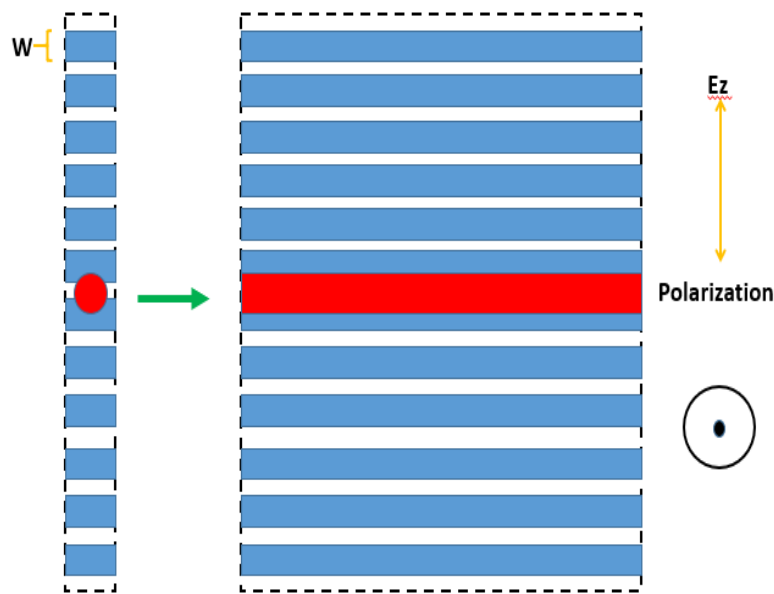


Fig. 5.1 Schematic of straight-line focus

X-axis direction. As shown in Fig 5.1 (It is a top view of this 3-D lens), the incident light is polarized in Y-axis direction and the direction of source is perpendicular to this paper. Since the incident light is polarized in Y-axis and we just switch the W to control the phase match, extending the length in X-axis direction will not give large influence about focus efficiency in theory.

Based on this idea, we had designed a 3-D lens with size $10\ \mu\text{m} \times 10\ \mu\text{m}$. In this design, the pitch size (period) is 150 nm, NA is 0.98, h is 420 nm, the value of refractive index n equals 2.12. As shown in Fig 5.2(a), it is the top view of the schematic of this 3-D lens which

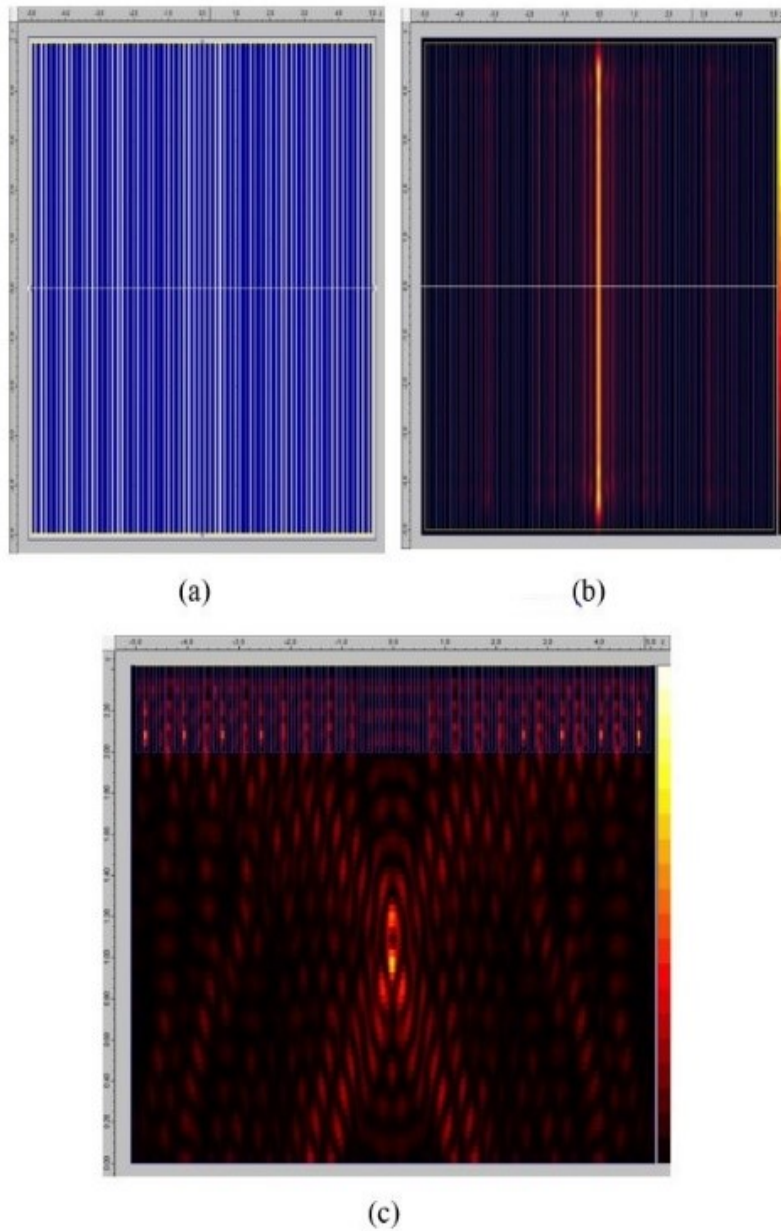


Fig. 5.2 (a) Schematic of straight-line focus metalens. (b) Field distribution at the focus layer. (c) Field distribution of side view.

can give a line focus. Fig 5.2(b) shows the field distribution under light incidence of 360 nm in one layer which includes the focus. As shown in Fig 5.2(c), it is the side view of field distribution at the middle of this lens. According to this field distribution in Fig 5.2(c), we are able to extract the layer we need to observe the shape of focus. So, it is clear that the reason we selected a relatively high numerical aperture is that it is easier for us to observe smaller size focus in different layers. As can be observed in Fig 5.2(b), the focus is clear and smooth concentrating profile proving that our idea to achieve line focus is feasible.

5.2 Several Methods to Approach ‘M’ Structure Gradually

In last chapter, we are able to make a ‘line’ focused by a 3-D lens. According to this progress, we want to utilize four lenses to achieve a ‘M’ structure. As shown in Fig 5.3, the ‘M’ is just like the logo of University of Michigan, composed by four lines. As we can imagine that if we just utilize our result in last chapter directly to compose a ‘M’ (each line is given by a lens), there will be some overlap between each lens. And the overlapping of structure may cause nano fabrication issue.

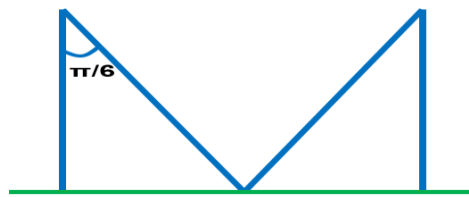


Fig. 5.3 ‘M’ structure

Focus away from symmetry axis: In this case, we need to design a kind of lens which can shift the position of its focus and then place these lenses at different location to achieve ‘M’. As shown in Fig 5.4, the focus is shifted from O to O' , C is the center of this lens and S is the length of this focal shift. The phase match condition can be described by the equation below. After several steps of simplification, we can obtain equation 5.2.1 which describes the requirement of phase shift to achieve the focus at point O' . In addition, equation 5.2.2 is for the phase condition that the focus would be shifted to the left side of this lens.

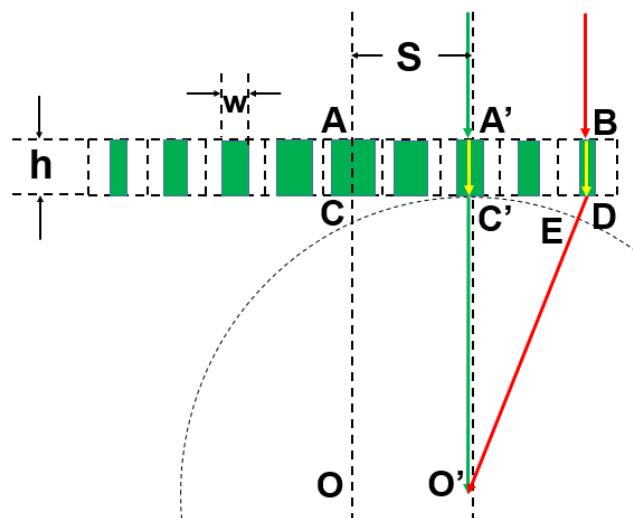


Fig. 5.4 Schematic of focus shift in X-axis direction

$$\text{Phase Shift} = \varphi(D) - \varphi(B) = 2\pi \times ED/\lambda$$

$$\text{Phase Shift} = \varphi(D) - \varphi(B) = 2\pi \frac{\sqrt{f^2 + C'D^2} - f}{\lambda}$$

$$\text{Phase Shift} = \varphi(D) - \varphi(B) = 2\pi \frac{\sqrt{f^2 + (X-S)^2} - f}{\lambda} \quad (5.2.1)$$

$$\text{Phase Shift} = \varphi(D) - \varphi(B) = 2\pi \frac{\sqrt{f^2 + (X+S)^2} - f}{\lambda} \quad (5.2.2)$$

With these two equations, we can design lenses with the function of focusing light at a

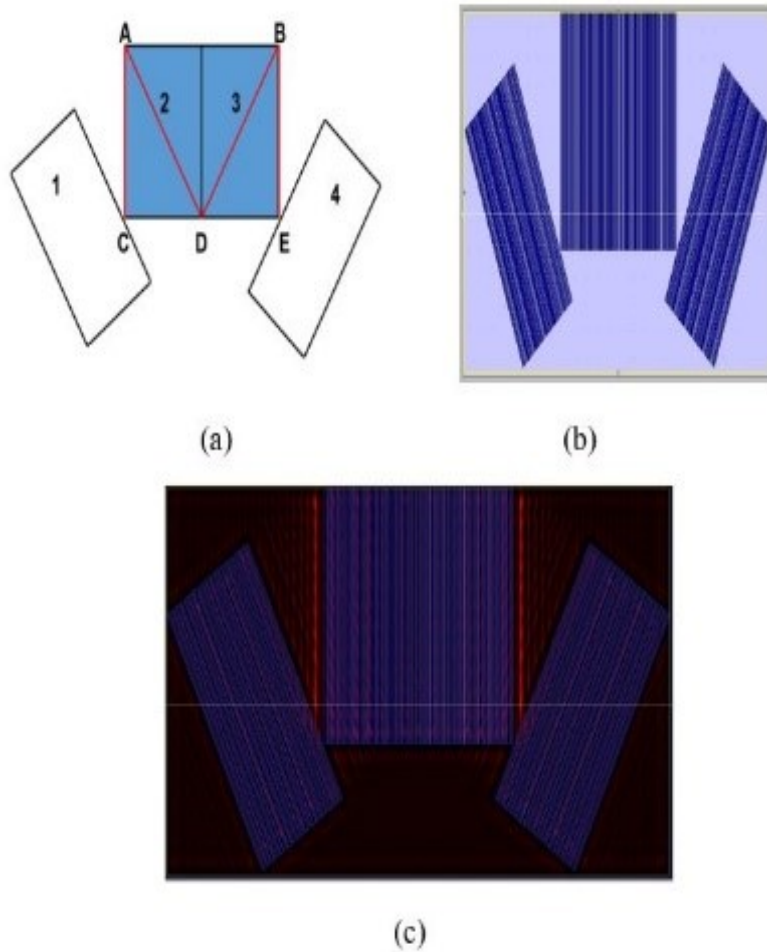


Fig. 5.5 Schematic of focus shift in X-axis direction

focal point away from its symmetry axis, even out of the diameter of the lens. In this study, we will propose and illustrate several ideas to achieve ‘M’ focus.

Four lenses with lined focus: As shown in Fig 5.5(a), lens 1 is used to achieve the focus line AD; lens 2 is designed to achieve the focus line AC; lens 3 is used to achieve the focus line BE; lens 4 is designed to achieve the focus line BD. Fig 5.5(b) is the design of metalens in our simulation software. Fig 5.5(c) shows the field distribution at the layer of focus under light incidence of 360 nm. As we can observe in Fig 5.5(c), lens 2 and lens 3 can achieve the focus line AC and BE, but there is no focus at AD and BD which does not achieve our desired results. The main reason is that we had rotated the angle of these phase shifters from 0 to $\pi/6$, making these phase shifters not perpendicular to the direction of incident light polarized. And then the focus efficiency was reduced. Although this idea is not successful, it supports our study result in chapter 4.

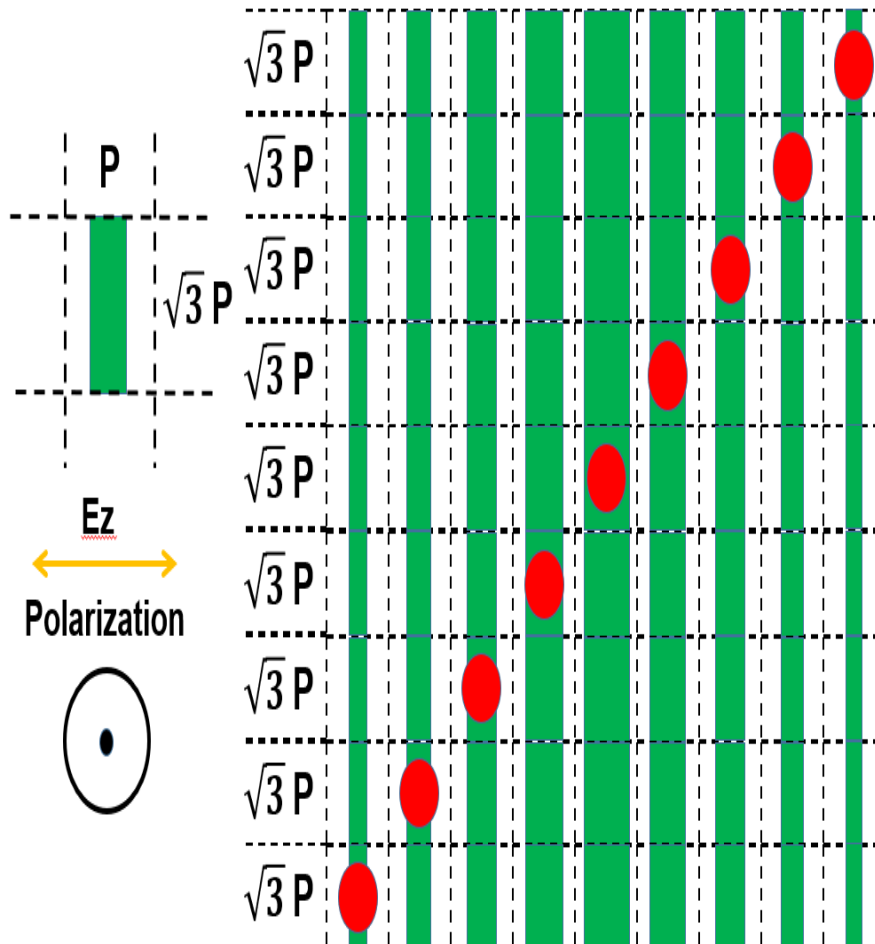
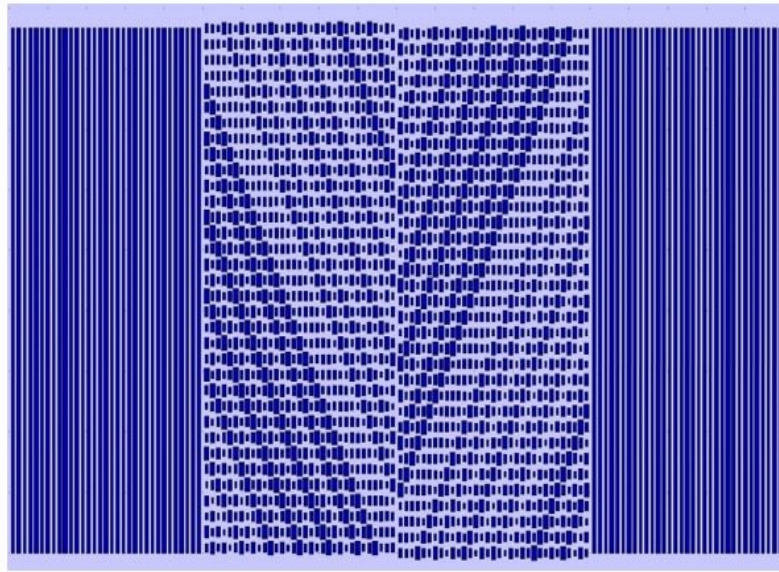
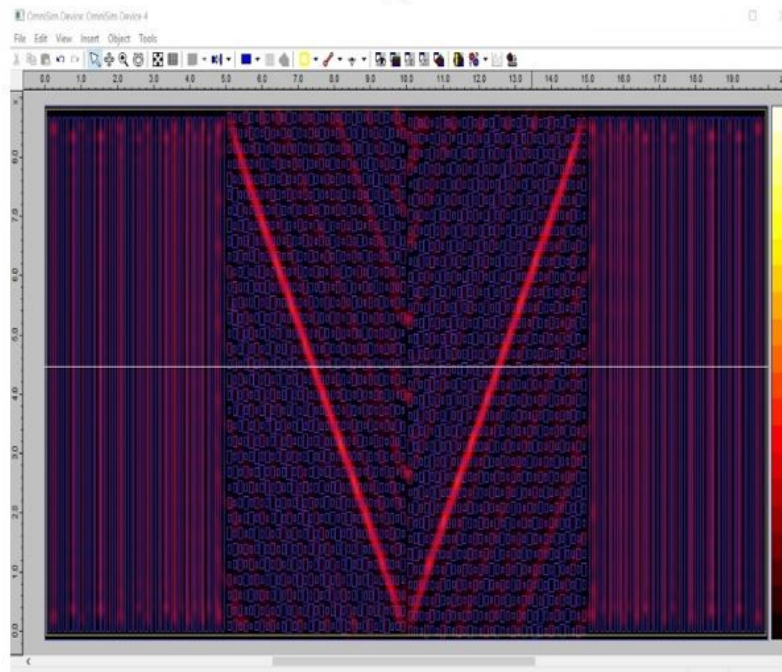


Fig. 5.6 Schematic of discretization method

Discretization method and application: Since we can't obtain a lined focus with positions in X-axis direction, these focal points are connected into a slash line. As shown in



(a)



(b)

Fig. 5.7 Simulation of discretization method

Fig 5.6, it is a top view of a 3-D lens; each red round represents the focus point achieved by nonzero angle by long strip phase shifters. We discretize this 3-D lens along the longitudinal direction, making it combined by multiple 2-D lenses, each lens has a focus at different each

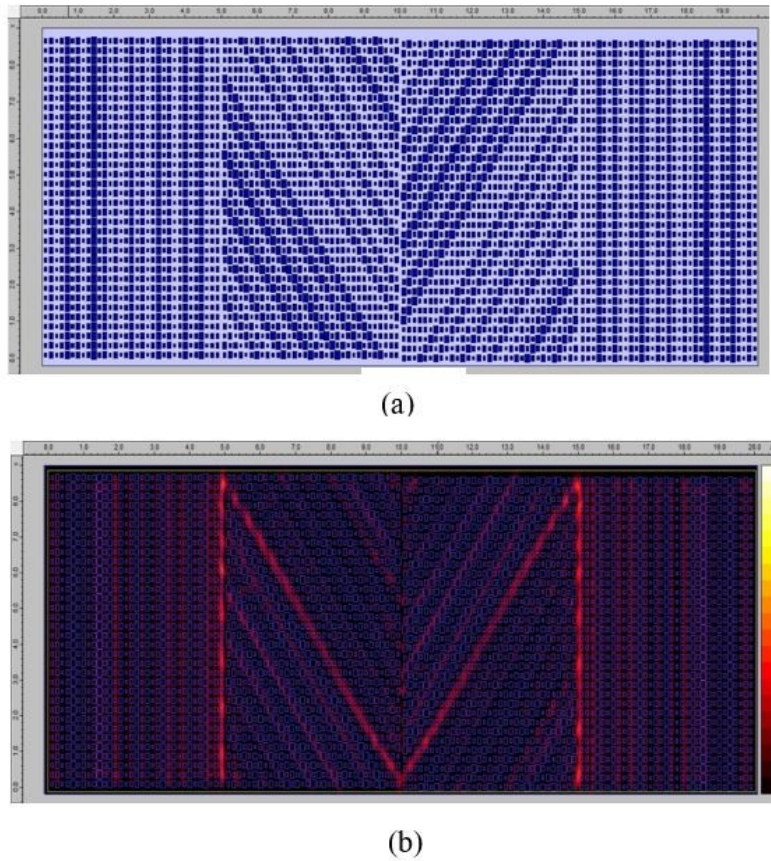


Fig. 5.8 Simulation of discretization method

2-D lens in X-axis direction. Since we need to obtain a lined focus with the angle of $\pi/6$ to compose ‘M’, we define the lattice with a length of $\sqrt{3} P$ (P is the value of period in X-axis direction) and a width of P .

According to this discretization method, we designed a lens in Fig 5.7 (a) combined by four lenses, including two lenses composed by long strip phase shifters and two lenses designed by discretization method. The reason we can just see a ‘V’ type focus in Fig 5.7 (b) is that the focal length of lenses designed by two different mechanism have a little difference. So, the lined focus given by long strip phase shifters is not in the same layer where we observed ‘V’. To solve this problem, we had designed a lens combined by four small lenses all designed by discretization method, shown in Fig 5.8(a). As we can observed in Fig 5.8(b), we finally had achieved ‘M’ structure.

Space saving design of ‘M’: Although we achieved ‘M’ structure by discretization method, we have to utilize four lenses which is space-consuming. So, we want to find a way

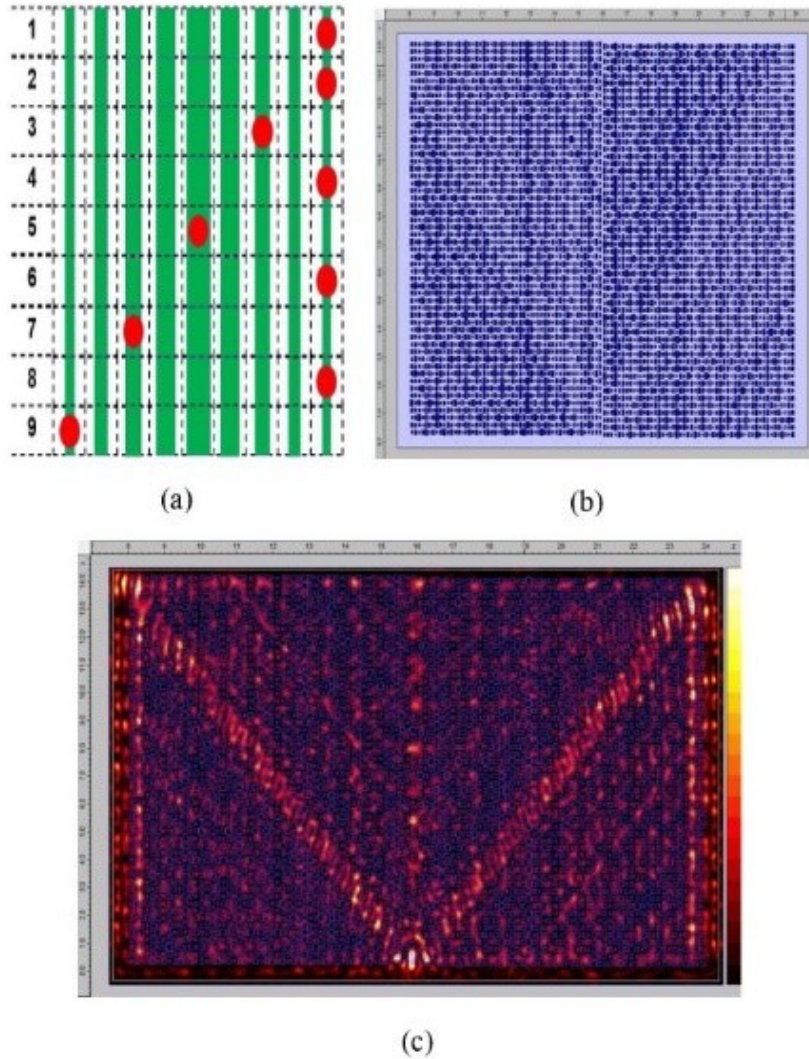


Fig. 5.9 Simulation of space saving design

to achieve two lined focus just by utilizing one lens. Based on our idea of discretization method, we marked each of the discrete horizontal lines with a sequence number and then divided them in parity (odd and even). The lines with odd serial number are used to implement the slash line focus, and the lines with even number are used to achieve vertical lined focus. Fig 5.9(a) illustrates the schematic of this idea. Fig 5.9(b) shows the design of the lens combined by two small lenses with size $8 \mu\text{m} \times 14 \mu\text{m}$. As we can observed in Fig 5.9(c), the filed distribution at 360 nm incidence shows that the focus ‘M’ is a little bit weaker and rougher than the focus in Fig 5.8(b). This is because the period of phase shifter is not small enough that gives large gap between each focus point. As we had analyzed in previous chapters, the period of phase shifter is depended on the wavelength of incident light. So, this idea about space saving can be utilized to shorter wavelength metalens in the future.

5.3 Two kinds of Arcuated Focus

Discretization method: Based on the idea of discretization, we have tried to complete a metalens with arcuated structure focus. Since this structure is a little bit complex and can be divided to four parts, we just propose a quarter arc structure. Since we had already figured out the mechanism and formula of straight-line focus lens, we want to make some modification based on this lens to achieve the arcuated focus lens. As shown in Fig 5.10(a), we assume that initially it was a straight-line focus lens which is composed by a lot of 2-D lenses, achieving a lined focus on symmetry axis (shown by yellow dotted line). And the black arcuated line shows the positions of each focus point we want to achieve by each 2-D lens. In Fig 5.10(a), Q is a random intersection point of the radius and arc, QO is radius. According to the focus position shift mechanism we proposed in equation 5.2.1 in chapter 5.2, we need to figure out the distance between point C and point Q and illustrate this value by a function of Y. We planned to write a matlab program to calculate the value of focus shift of each 2-D lens at

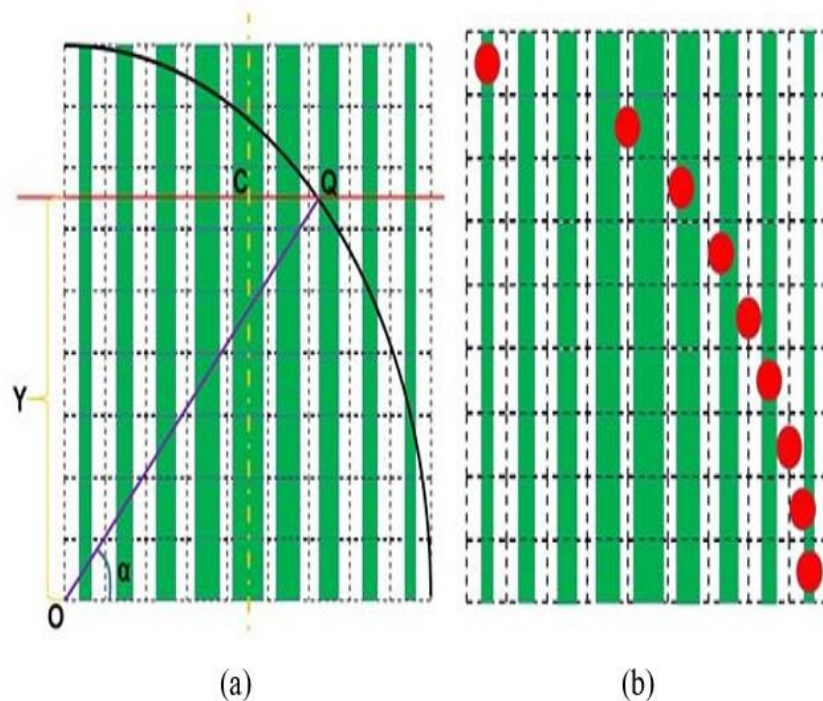


Fig. 5.10 Schematic of arcuated focus lens

different ordinate positions (Y). After some basic calculation, the focus shift CQ can be described in equation 5.3.1. Then we combine equation 5.3.1 and 5.2.1 to figure out equation 5.3.2, describing the phase shift requirement at each location of this 3-D lens.

$$CQ = \sqrt{OQ^2 - Y^2} - OQ/2 \quad (5.3.1)$$

$$Phase\ Shift = \varphi(D) - \varphi(B) = 2\pi \frac{\sqrt{f^2 + (X - (\sqrt{OQ^2 - Y^2} - \frac{OQ}{2}))^2} - f}{\lambda} \quad (5.3.2)$$

With this formula, we had designed a schematic of this lens shown in Fig 5.10(b), the red rounds represent focus point achieved by this design. As we can observed in Fig 5.10(b), the density of these focus points is lower when the value of Y is lager. This is because the absolute value of the slope of this arc is becoming larger when the value of Y increases. Fig 5.11(a) shows the design of this arcuated focus lens with size $8\ \mu\text{m} \times 8\ \mu\text{m}$ and $NA = 0.95$; and the simulation result at 360 nm incidence of filed distribution is shown in Fig 5.11(b). Obviously, the result of the simulation highly supports our theoretical analysis. Although this method seems not very suitable for making arcuated focus, we can increase the density of these focus points by shrinking the pitch size (period) of each individual phase shifter to solve this problem in a certain extent.

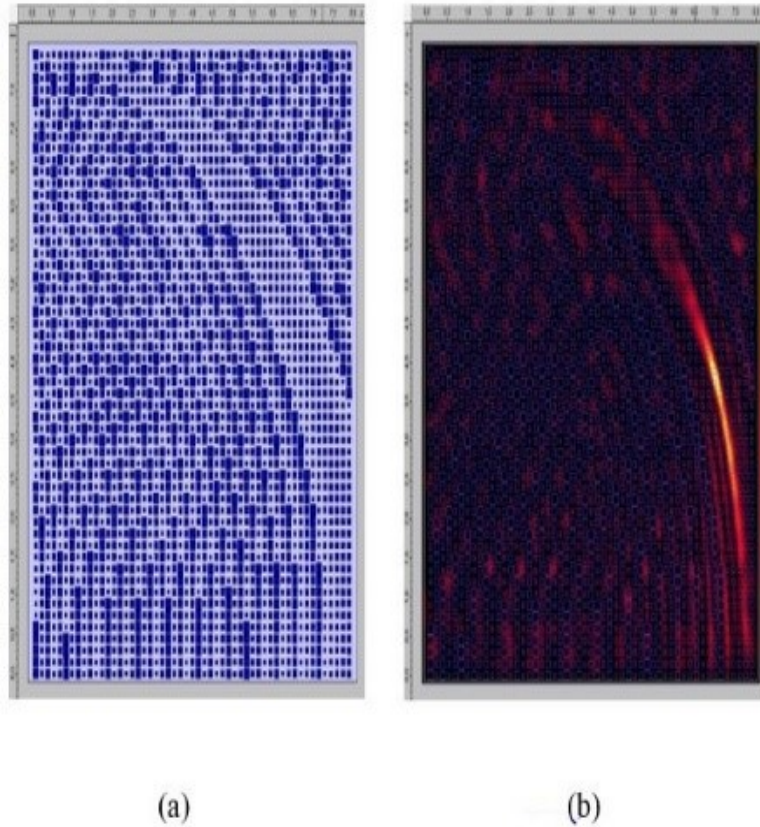


Fig. 5.11 Simulation of arcuated focus lens

Rotation method: Due to the defect and limitation of discretization method, we tried to find out something in grating structure. This grating based metalens with $NA = 0.99$ is designed by rotating the 2-D phase profile along its far right with diameter of $12\ \mu\text{m}$. If we

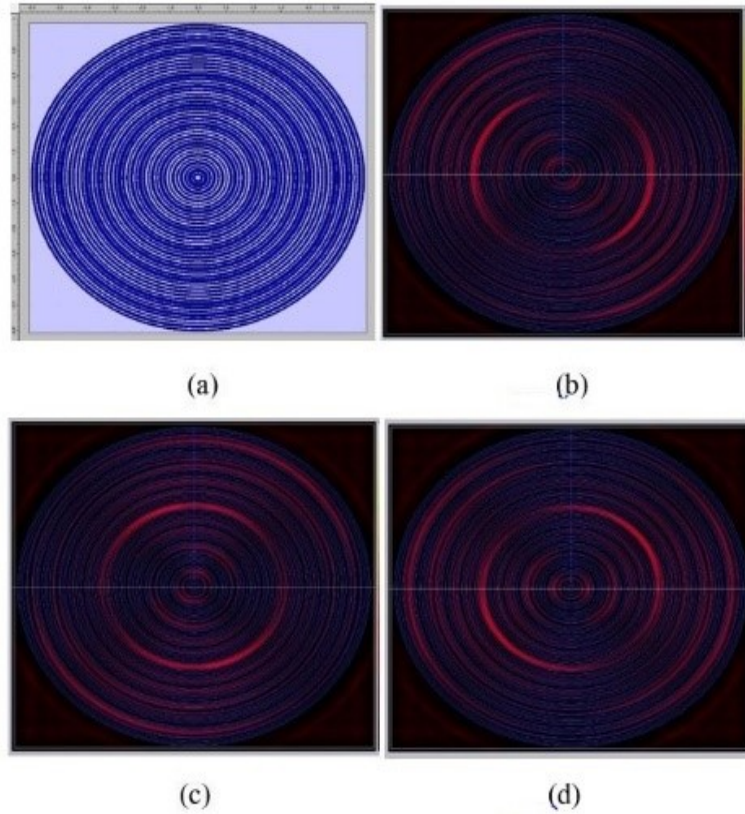


Fig. 5.12 Design and Simulation of arcuated focus lens

make the rotation along the 2-D lens's central, the focus will be a point as we described in Fig 3.9 in chapter 3.3. In the simulation, we utilized a circularly polarized incidence of 360 nm. As can be observed in Fig 5.12 (b) (c) (d), the focus was rotating figure by figure. This is because we made these screen captures at different time. It also proves that grating lens is able to provide the same focus efficiency for light incidence polarized in any direction.

Chapter VI Conclusion

This thesis mainly introduced the leading-edge theory and three topics of Metalens completed by the author, with background introduction of Metalens and Finite Difference Time Domain (FDTD) method in electromagnetism. The conclusion for each chapter is briefly summarized at the end of each chapter. As the overall conclusion, here a summary of the entire thesis is stated. In chapter two we illustrated the derivation of the theory in a step-by-step manner, clearly showing how metalens come from and why we need to study in metalens. The design of metalens in chapter three is proposed with two parts, the RCWA method to design metalens, and the simulation result and optical characterization with analysis about the relationship between the pitch size and focus efficiency. Chapter four proposed the first time a metalens is designed with the ability to distinguish linear polarization while maintaining concentrating performance. Finally, we illustrated several kinds of metalens providing focus with different shapes and a space saving method which is valuable for the further study.

REFERENCES

- [1] M. Ye, V. Ray, and Y. Yi, "Achromatic Flat Subwavelength Grating Lens Over Whole Visible Bandwidths," *IEEE Photon. Technol. Lett.*, vol. 30, pp. 955-958, May. 2018.
- [2] M. Ye, X. Guo and Y. Yi, "Transmission enhancement of subwavelength grating microlens by tapered nanostructure," *MRS Commun*, vol. 8, pp. 509-513, June. 2018.
- [3] S. Jahani and Z. Jacob, "All dielectric metamaterials," *Nature Nanotechnology*, vol. 11, pp. 23-36, 2016.
- [4] P. R. West, J. L. Stewart, A. V. Kildishev, V. M. Shalaev, V. V. Shkunov, F. Strohkendl, Y. A. Zakharenkov, R. K. Dodds, and R. Byren, "All-dielectric subwavelength metasurface focusing lens," *Opt. Express*, vol. 22, pp.26212-26221, 2014.
- [5] Y. Wang, J. Miao, Y. Tian, C. Guo, J. Zhang, T. Ren, and Q. Liu, "TiO₂ micro-devices fabricated by laser direct writing," *Opt. Express*, vol. 19, pp.17390-17395, 2011.
- [6] A. Asadollahbaik, S. A. Boden, M. D. B. Charlton, D. N. R. Payne, S. Cox and D. M. Bagnall, "Reflectance properties of silicon moth-eyes in response to variations in angle of incidence, polarization and azimuth orientation," *Opt. Express*, vol. 22, pp. A402-A415, 2014.
- [7] P. Pignalosa, B. Liu, H. Chen and Y. Yi, "Giant light extraction enhancement of medical imaging scintillation materials using bio inspired integrated nano structures," *Optics Letters*, vol. 37, pp. 2808, 2012.
- [8] F. Saffih, C. Con, A. Alshammari, M. Yavuz, and B. Cui, "Fabrication of silicon nano structures with large taper angle by reactive ion etching," *J. Vac. Sci. Technol*, vol. B 32, pp. 06F1104-1, 2014.
- [9] F. Lu, F. G. Sedgwick, V. Karagodsky, C. Chase, and C. G. Chang-Hasnain, "Planar high-numerical-aperture low-loss focusing reflectors and lenses using subwavelength high contrast gratings," *Opt. Express.*, vol. 18, pp. 12606-12614, June 2010.
- [10] C. J. Chang-Hasnain, "High-contrast gratings as a new platform for integrated optoelectronics," *Semicond. Sci. Technol.*, vol. 26, pp. 014043, Dec. 2011.
- [11] D. Fattal, J. Li, Z. Peng, M. Fiorentino, and R. G. Beausoleil, "Flat dielectric grating reflectors with focusing abilities," *Nature Photonics.*, vol. 4, pp. 466-470, May. 2010.
- [12] X. Duan, G. Zhou, Y. Huang, Y. Shang, and X. Ren, "Theoretical analysis and design guideline for focusing subwavelength gratings," *Opt. Express.*, vol. 23, pp. 2639-2646, Feb. 2015.
- [13] S. He, Z. Wang, Q. Liu, and W. Wang, "Study of focal shift effect in planar GaN high contrast grating lenses," *Opt. Express*, vol. 23, pp. 29360-29368, Nov. 2015.

- [14] M. Ye, X. Guo and Yi. Y, “Transmission enhancement of subwavelength grating microlens by tapered nanostructure,” *MRS Communications*, vol. 8, pp. 509-513, June 2018.
- [15] W. Stork, N. Streibl, H. Haidner, and P. Kipfer, “Artificial distributed-index media fabricated by zero-order gratings,” *Opt. Lett.*, vol. 16, pp. 1921-1923, Dec. 1991.
- [16] M. Ye and Y. Yi, “Subwavelength grating microlens with taper-resistant characteristics,” *Opt. Lett.*, vol. 42, pp. 1031-1034, Mar. 2017.
- [17] M. Khorasaninejad, W. T. Chen, R. C. Devlin, J. Oh, A. Y. Zhu, and F. Capasso, “Metalens at visible wavelengths: Diffraction-limited focusing and subwavelength resolution imaging,” *Science*, vol. 352, pp. 1190, June 2016.
- [18] J. P. B. Mueller, N. A. Rubin, R. C. Devlin, B. Groever, and F. Capasso, “Metasurface Polarization Optics: Independent Phase Control of Arbitrary Orthogonal States of Polarization,” *Physical Review Letters*, vol. 118, pp. 113901, Mar. 2017.
- [19] M. Khorasaninejad, A. Y. Zhu, C. Roques-Cames, W. T. Chen, J. Oh, I. Mishra, R. C. Devlin, and F. Capasso, “Polarization-Intensive Metalenses at Visible Wavelengths,” *Nano Lett.*, vol. 16, pp. 7229-7234, Oct. 2016.
- [20] Z. Fan, Z. Shao, M. Xie, X. Pang, W. Ruan, F. Zhao, Y. Chen, S. Yu, and J. Dong, “Silicon nitride metalenses for unpolarized high-NA visible imaging,” in *Proc. of the 2018 Conference on Lasers and Electro-Optics*, 5-10 May 2018, San Jose, CA, USA.
- [21] H. V. Jansen, M. J. Boer, R. J. Wiergerink, N. R. Tas, E.J.T. Smulders, C.R. Rusu, and M. C. Elwenspoek, “RIE lag in high aspect ratio trench etching of silicon,” *Microelectronic Engineering*, vol. 35, pp. 45-50, Feb. 1997.
- [22] M. Ye and Y. Yi, “Influence of grating thickness in low-contrast subwavelength grating concentrating lenses,” *Optical Engineering*, vol. 55, pp. 075102, July, 2016.
- [23] N. Yu, P. Genevet, M. A. Kats, F. Aieta, J. Tetienne, F. Capasso, Z. Gaburro, “Light Propagation with Phase Discontinuities: Generalized Laws of Reflection and Refraction,” *Science*, vol. 334, pp. 333-337, Oct. 2011.
- [24] S.O.Kasap, “*Optoelectronics and Photonics Principles and Practices*,” Second Edition, Retrieved from <https://pdfread.org>.

Appendix: Publications

Conference:

[1] Y. Yi, W. Guo and Y. Peng, 'Enhancement of Light Trapping for Thin-Film Silicon Solar Cells', MRS Advances, MRSAdv-2018-3037668.R1 (accepted for publication)

Journal:

[1] M. Ye, V. Ray, Y. Peng, W. Guo and Y. Yi, 'Linear Polarization Distinguishing Metalens in Visible Wavelength', Optics Letters, 347529 (accepted for publication)

[2] M. Ye, Y. Peng and Y. Yi, 'Silicon-rich Nitride Thin Films for Emerging Metalens Fabrication', Optical Materials Express, 348197 (received successfully)